



**NAVFAC**  
Naval Facilities Engineering Command

ENGINEERING SERVICE CENTER  
Port Hueneme, California 93043-4370


**TECHNICAL REPORT**  
**TR-2295-AMP**

**ASSESSMENT OF PROPOSED WAVE BARRIERS  
FOR 5T SMALL BOAT BASIN AT NAVAL STATION  
NORFOLK VIRGINIA**

July 2008

By:  
Erick T. Huang, PhD, PE  
Hamn-Ching Chen, PhD, PE

Approved for public release; distribution is unlimited.

 Printed on recycled paper

**REPORT DOCUMENTATION PAGE**

*Form Approved  
OMB No. 0704-0811*

The public reporting burden for this collection of information is estimated to average 1 hour per response, including the time for reviewing instructions, searching existing data sources, gathering and maintaining the data needed, and completing and reviewing the collection of information. Send comments regarding this burden estimate or any other aspect of this collection of information, including suggestions for reducing the burden to Department of Defense, Washington Headquarters Services, Directorate for Information Operations and Reports (0704-0188), 1215 Jefferson Davis Highway, Suite 1204, Arlington, VA 22202-4302. Respondents should be aware that notwithstanding any other provision of law, no person shall be subject to any penalty for failing to comply with a collection of information, if it does not display a currently valid OMB control number.

**PLEASE DO NOT RETURN YOUR FORM TO THE ABOVE ADDRESS.**

1. REPORT DATE (DD-MM-YYYY)			2. REPORT TYPE		3. DATES COVERED (From - To)	
4. TITLE AND SUBTITLE ASSESSMENT OF PROPOSED WAVE BARRIERS FOR 5T SMALL BOAT BASIN AT NAVAL STATION NORFOLK VIRGINIA					5a. CONTRACT NUMBER	
					5b. GRANT NUMBER	
					5c. PROGRAM ELEMENT NUMBER	
6. AUTHOR(S) Erick T. Huang, NAVFAC ESC Hamn-Ching Chen, Texas A&M University					5d. PROJECT NUMBER	
					5e. TASK NUMBER	
					5f. WORK UNIT NUMBER	
7. PERFORMING ORGANIZATION NAME(S) AND ADDRESSES NAVFAC ESC 1100 23 <sup>rd</sup> Ave, Port Hueneme CA 93043-4370					8. PERFORMING ORGANIZATION REPORT NUMBER	
9. SPONSORING/MONITORING AGENCY NAME(S) AND ADDRESS(ES) Port Operations, US NAVSTA Norfolk, Virginia 1837 Morris Street, Building Z133 Norfolk VA 23511					10. SPONSOR/MONITORS ACRONYM(S)	
					11. SPONSOR/MONITOR'S REPORT NUMBER(S)	
12. DISTRIBUTION/AVAILABILITY STATEMENT Approved for public release; distribution is unlimited.						
13. SUPPLEMENTARY NOTES						
14. ABSTRACT This task assesses the dynamic responses of a small boat basin to local storms and quantifies the performance of a proposed breakwater. The assessment procedure adopts a sophisticated Computational Fluid Dynamic model capable of preserving the exact site condition and all prevailing hydrodynamic mechanisms at high accuracy. This exercise clearly illustrates the feasibility and merits of modern simulation models for designs. The results confirm that this basin is sensitive to local storms. It is particularly susceptible to oblique seas. The present breakwater setup with the north arm alone is insufficient to shelter the basin. The proposed south arm is essential. Two breakwaters combined work reasonably well in perpendicular waves, however, lose its effectiveness in oblique seas. Two simple measures of high potential to further mitigate wave disturbances inside the basin deserve considering. One is to slightly extend the south breakwater and bend its north end by 45 degrees to the east. This would reduce the amount of wave penetration through the basin entrance in oblique seas. In fact, the south breakwater need not be straight or parallel to the north breakwater. A zigzag shape may be more favorable from the perception of basin stability. The other is to install a wave absorbing mechanism along the south bulkhead and the weather side of the north breakwater and perhaps the leeward side of the south breakwater as well. This would reduce wave intrusions via successive reflections off the breakwaters and the south bulkhead.						
15. SUBJECT TERMS Wave transformation; breakwaters, irregular sea bed; small boat basin; harbor oscillations; chimera method						
16. SECURITY CLASSIFICATION OF:			17. LIMITATION OF ABSTRACT	18. NUMBER OF PAGES	19a. NAME OF RESPONSIBLE PERSON	
a. REPORT	b. ABSTRACT	c. THIS PAGE			19b. TELEPHONE NUMBER (include area code)	
U	U	U				

## EXECUTIVE SUMMARY

The 5T Basin is a small boat basin located behind the main bulkhead along the waterfront of Naval Station Norfolk (NAVSTA Norfolk), Virginia. The original design of this basin had a pair of breakwaters at the entrance<sup>1</sup>. Budget concerns resulted in the south arm being deleted at the previous phase. The most recent plan is to reinstate this feature. A new design of the south arm was slated for construction in March 2008. However, existing data are insufficient to confirm the effectiveness of this breakwater. The Port Operations of NAVSTA Norfolk tasked the Naval Facilities Engineering Service Center (NAVFAC ESC) to quantify the performance of this breakwater in early February 2008<sup>2</sup>. This assignment involves a thorough analysis of wave transformation in a complex coastal ambience of irregular shoreline and sea bed bathymetry.

The analysis adopts an advanced Computational Fluid Dynamic (CFD) simulation model built on a three-dimensional potential flow numerical method. This method solves the Laplace equation for unsteady body-wave couplings using a chimera domain decomposition approach. This simulation model addresses the exact site conditions in full detail and therefore faithfully preserves all hydrodynamic mechanisms at high accuracy. The simulation results provide a high resolution time history of the entire flow field. This allows developers to extract essential design data and trace the causes of specific events for prudent engineering decisions.

The results confirmed that the north breakwater alone is insufficient to protect the 5T Basin from local storms. This basin, as is, observes wave disturbances as high as 90 percent of the incident waves, or exceeding 150 percent under certain conditions. The addition of the south breakwater cuts the disturbances by 60 percent from the present level. The proposed breakwater layout works well for waves approaching from the west (roughly perpendicular to the breakwaters), yet gradually loses its effectiveness as the wave heading swings toward the northwest.

This effort recommends consideration of two simple measures with high potential to further mitigate wave disturbances inside the basin. One is to slightly extend the south breakwater and bend its north end by 45 degrees to the east. This would reduce the amount of wave penetration through the basin entrance in oblique seas. In fact, the south breakwater need not be straight or parallel to the north breakwater. A zigzag shape may be more favorable from the perception of basin stability. The other is to install wave absorbing mechanisms along the south bulkhead as well as the weather side of the north breakwater and perhaps the leeward side of the south breakwater. This would reduce wave intrusions via successive reflections off the breakwaters and the south bulkhead, and reduce the potential to induce cross-basin oscillations.

---

<sup>1</sup> See [Figure 2](#) of the main text.

<sup>2</sup> This work was partly sponsored by Ms. Sandra Hawkinson of the Port Operations of U.S. Naval Base Norfolk and Mr. Joseph Piper of NAVFAC Atlantic Division under Work Order N6247008WRA0038.

## TABLE OF CONTENTS

	<b>Page</b>
<b>BACKGROUND</b> .....	1
<b>SCOPES</b> .....	1
<b>THEORETICAL CONSIDERATIONS</b> .....	4
Simulation Code.....	4
Numerical Model .....	5
<b>MODEL SETUP</b> .....	7
Basin and structure layouts .....	7
Numerical Basin.....	9
Sea Bed .....	9
Grid System .....	10
Incident waves .....	13
<b>RESULTS</b> .....	17
Wave activities without the south breakwater .....	17
Wave activities with south breakwater .....	25
<b>SUMMARY</b> .....	38
<b>RECOMMENDATIONS</b> .....	40
<b>REFERENCES</b> .....	41

## LIST OF FIGURES

	Page
Figure 1. Location map and basin layouts. ....	3
Figure 2. General layout of the proposed breakwater.....	3
Figure 3. (a) Paths of wave propagation and (b) ring wave patterns .....	4
Figure 4. Sketch of overall plan of 5T Basin .....	8
Figure 5. (a) Field confirmations of basin geometry, (b) numerical representations..	8
Figure 6. Echo sounding chart of 5T Basin .....	9
Figure 7. (a) Sea bed bathymetry, (b) floating docks, and (c) sea bed profiles. ....	10
Figure 8. (a) block layouts, (b) wave maker, and (c) grid systems.....	12
Figure 9. (a) models for various wave headings and (b) periods.....	13
Figure 10. Incident waves of 4, 6, and 8 seconds .....	14
Figure 11. Example of incident waves of 4 seconds from 0° heading .....	14
Figure 12. Wave distribution without south breakwater (prd= 4 sec, hdg=00 deg) ..	19
Figure 13. Diffraction pattern through a gap of five wave lengths, Johnson (1952). 19	
Figure 14. Standing waves in front of bulkheads .....	20
Figure 15. Cross Basin oscillations.....	20
Figure 16. Wave distribution without south breakwater (4 sec, 22.5 deg) .....	21
Figure 17. Wave distribution without south breakwater (4 sec, 45 deg) .....	21
Figure 18. Wave distributions without the south breakwater (6 sec. 00 deg).....	23
Figure 19. Wave distributions without the south breakwater (8 sec. 00 deg).....	23
Figure 20. Sensitivity of wave lengths without the south breakwater .....	24
Figure 21. Wave distribution with the south breakwater (4 sec, 00 deg) .....	29
Figure 22. Diffraction diagram around a semi-infinite barrier .....	29
Figure 23. Wave distribution with the south breakwater (4 sec, 22.5 deg) .....	30
Figure 24. Wave distribution with the south breakwater (4 sec, 45 deg) .....	30
Figure 25. Summary of breakwater performances in local storms .....	31
Figure 26. Wave distributions with the south breakwater (6 sec. 00 deg).....	31
Figure 27. Wave distributions with the south breakwater (8 sec. 00 deg).....	32
Figure 28. Sensitivity of breakwater performance to wave lengths.....	32
Figure 29. Sensitivity of wave lengths with the south breakwater .....	33
Figure 30. Resonance-like waves behind the south breakwater (8 sec) .....	33
Figure 31. Resonance-like waves behind the south breakwater (6 sec) .....	34
Figure 32. Resonance-like actions behind the south breakwater (4 sec) .....	34
Figure 33. Sensitivity of resonance-like oscillations to wave periods r .....	35
Figure 34. Breakwater changes wave nature in the basin (00 deg. 8 sec.) .....	35
Figure 35. Breakwater changes wave nature in the basin (00 deg. 6 sec.) .....	36
Figure 36. Breakwater changes wave nature in the basin (00 deg. 4 sec.) .....	36
Figure 37. Wave activities near the floating docks (without south breakwater) .....	37
Figure 38. Wave activities near the floating docks (with south breakwater).....	37
Figure 39. Potential measures to mitigate wave activities inside the basin .....	40

## **BACKGROUND**

The 5T Basin is a small indentation behind the main bulkhead of NAVSTA Norfolk Waterfront between Pier 5 and Pier 6 as shown in [Figure 1](#). This basin is mainly of rectangular shape, surrounded by straight bulkheads on three borders, and linked to the waterfront via an entrance at its western side. Its long axis of this basin points roughly 15 degrees south of due west. The original design of the basin had a pair of breakwaters at the entrance, one running from the northern bulkhead toward the south and the other running from the south bulkhead to the north as illustrated in [Figure 2](#). Budget concerns resulted in the south arm being deleted from the project at the previous phase, leaving the basin partly exposed to wind waves approaching from the west to the northwest. The basin, as such, suffers substantial wave turmoil during storms. The most recent plan is to reinstate the south breakwater. However, concerns remain whether these two breakwaters would provide sufficient sheltering to the basin as planned. Naval Facilities Engineering Service Center (NAVFAC ESC) was tasked by the Port Operations of NAVSTA Norfolk to assess the consequence of implementing the second breakwater. A high fidelity Computational Fluid Dynamic (CFD) model developed by NAVFAC ESC in conjunction with Texas A&M University (TAMU) was used to trace the wave activities around and inside the basin with or without the second breakwater. The efficiency of the second breakwater can be readily evaluated with high confidence based on a complete database. This model performs like a numerical towing tank. It is capable of reproducing all activities expected from a physical test facility. It addresses physical events in their exact site circumstances beyond the details achievable by physical modeling. Its performance has been repetitively confirmed by laboratory and field measurements through previous applications in the past 15 years. The simulation results provide a comprehensive, seamless solution in three-dimensional space throughout the entire event.

## **SCOPES**

Wave activities in 5T Basin is dictated by many physical factors including:

- Nature of incident waves: periods, heights, and heading
- Basin geometry: shape, dimension, and sea bed bathymetry
- Nature of basin boundaries: slope, permeability, and rigidity
- Nature of pier facilities inside the basin: locations, sizes, and geometries
- Breakwater layout: location, length, shape, and orientation
- Layout of moored ships at the main waterfront
- Local wind conditions and tide elevations

In order to meet the prescribed construction schedule, this study considers only parameters essential to a fair assessment of the breakwater performance for decision making. Since the basin characteristics including geometry, boundary conditions, pier layouts, and bottom bathymetry are unlikely to change, and the proposed breakwater configuration looks reasonable, this analysis adopted all basin and breakwater particulars as described in the sponsor furnished documents. Winds, currents, and tides may slightly alter the process of wave transformations. Nevertheless, it is fair to compare breakwater

performances on a common background ambience of prescribed nature without losing much generality. The present study arbitrarily chose the instant of slack tide without wind or current. The simulation results only represent the wave activities induced by the set of incident waves in consideration, rather than the worst case situation 5T Basin may observe. However, influences of the default parameters may be addressed with minor revisions to the numerical model if time and resources permit.

For the inland water of Hampton Roads with limited fetch, daily recurrent extremes of local wind waves are estimated in the range of Sea State 3 with wave heights of 3 to 5 feet and associated peak periods of 4 to 6 seconds<sup>3</sup>. These waves are essentially linear and can be integrally represented by model waves of unit amplitude for practical purposes. Nevertheless, the present method is capable of handling nonlinear waves as demonstrated by Kang, Chen and Huang (1998) and Chen and Liu (2001) if wave activities due to extreme weathers are desired. As a result, the wave parameters can be further reduced to periods and headings. The present simulation selected a model wave of 4 seconds approaching from three headings at 0, 22.5, and 45 degrees north of the long axis of 5T Basin. Two additional cases were conducted with 6- and 8-second waves to explore the sensitivity of breakwater performance to wave periods.

The present study began with an initial sequence to address wave activities in the basin as is. The main purpose is to review the hydrodynamic nature of this basin and set a tangible baseline for subsequent analysis. The second sequence identifies the influences introduced by the south breakwater. Two sequences combined are expected to provide sufficient contrasts for breakwater performance assessment.

An additional feature, which is excluded from the present scope but may deserve some attentions, is the influence of moored ships along the waterfront. Since the basin is located between Pier 5 and Pier 6 (Figure 1), vessels at these piers may partially block or reflect the oblique incident waves into the basin. However, these ships integrally are more likely to ease than to enhance incident waves. Waves possibly bouncing off the ships at Pier 6 into the basin are approaching from southwest. Wave sources from this direction are mostly sheltered by Craney Island however. For brevity, this study chose to explore the worst condition when Piers 5 and 6 are fully open. The influences of the moored ships to wave activities in 5T Basin may be investigated later, if necessary.

This report consists of three parts presenting respectively: (a) simulation codes and numerical model setups, (b) simulation results and discussions, and (c) conclusions and recommendations. Since the wave activities inside the basin are highly dynamic and hardly reach steady-state within practical simulation durations in consideration, the results are also presented in movie clips wherever necessary. All figures and embedded movies may be activated by holding the <ctrl> key and clicking the link (in blue fonts) simultaneously<sup>4</sup>. These electronic images may be expanded for more details.

---

<sup>3</sup> As determined from Figure 3-24 of Shore Protection Manual using fetch length of 20 miles and wind speed of 30 MPH.

<sup>4</sup> <Ctrl> is not needed in PDF file.





Figure 1. Location map and basin layouts.

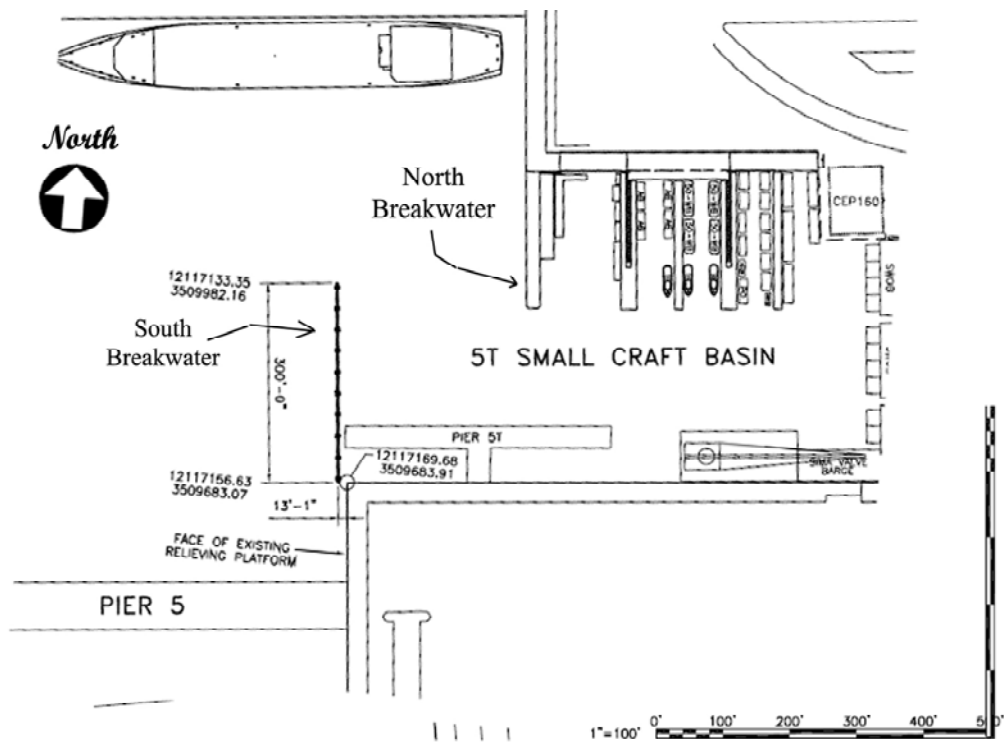


Figure 2. General layout of the proposed breakwater.



## THEORETICAL CONSIDERATIONS

Water waves transform once they touch the sea bottom or encounter physical boundaries. They change in height, profile, or heading as a result of energy redistribution in compliance to boundary constraints. Typical forms of transformation include reflection, refraction, and diffraction. Analytical solutions are available for regular waves coupling with simple structures in open water over sea bed of mild slopes. Linear superposition often provides fair approximations in such cases. However, the analysis procedure becomes tedious and labor intensive at true engineering sites of irregular water domain with complex sea bed and coastal structures like the ambience around 5T Basin. Note that incident waves may enter the basin via various paths. Waves entering via different paths couple and form complex, short-crest ring waves inside the basin as shown in Figure 3. In addition, the intruding waves continue to feed the basin and bounce around in endless loops inside. The asymmetric basin geometry and oblique wave heading tend to trigger various basin oscillations. Eventually, the trapped energy will top out the holding capacity of the basin and begin to escape via the basin entrance. Traditional analytical solutions normally overlook these induced mechanisms. A more sophisticated algorithm, like the present method, is desired to expose sufficient insights essential for effective decision making.

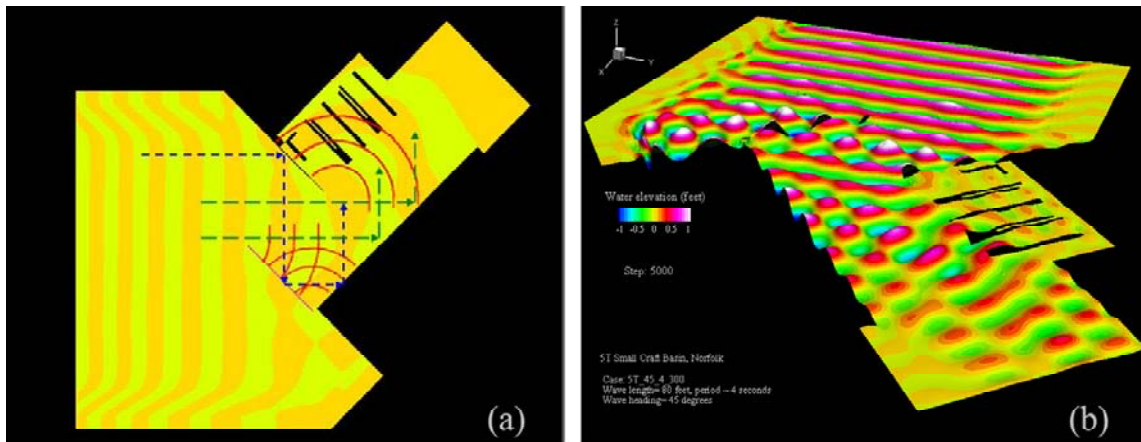


Figure 3. (a) Paths of wave propagation and (b) ring wave patterns.

### Simulation Code.

Chen and Lin (1998, 2000) established an efficient numerical algorithm, CHAMPS (CHimera finite Analytic Method Potential-flow Solver), to trace the transient wave fields around compound coastal structures in three-dimensional space. This algorithm solves the Laplace equation on structured multi-block grids using the finite-analytic method of Chen, Patel, and Ju (1990). Within each computational block, velocity potential was solved on a general curvilinear, body-fitted coordinate system.

CHAMPS assumes a chimera domain decomposition technique and attains a full compliance to physical realities of complex geometries. A highly irregular fluid domain may be divided into multiple blocks of convenience. Each block may be digitized

separately and subsequently linked by embedding, patching, or overlapping to form the ultimate computational domain. Selective grids may be refined in accordance with the nature of flow fields without a significant increase in total processing time. The chimera technique treats complex geometries and flow conditions across block boundaries by interpolations.

Chen and Lin (2000) demonstrated the above stated engineering merits of CHAMPS for wave transformations around compound coastal structures through a case study to quantify the performance of a conceptual breakwater system configured to shelter a large floating platform behind them. The results confirmed its capability to precisely catch all known wave activities observed around breakwaters, including reflection, refraction, and diffraction, as well as their superposition and cancellation couplings. Chen and Liu (2001) further demonstrated the precisions of this code for wave transformations around various coastal structures in deep or shoal waters of arbitrary depths. This CHAMPS code consistently reproduced the analytical solution of Dalrymple and Martin (1996) and experimental observations by Vincent and Briggs (1989) with exceptional accuracies.

### **Numerical Model.**

For the wave transformation analysis considered here, the associated boundary value problem can be constructed using a Cartesian coordinate system  $(x,y,z)$ . The incident waves generated by the wavemaker are traveling in the  $x$  direction, and the  $z$ -axis is pointing upward with  $z = 0$  representing the mean water surface. It is assumed that the fluid is incompressible and inviscid and that the flow is irrotational. This implies the existence of a velocity potential function  $\phi(x,y,z,t)$  such that the velocity can be described by  $\vec{V} = \nabla\phi$ . Due to the conservation of fluid mass, the velocity potential  $\phi$  satisfies the Laplace equation:

$$\nabla^2\phi = 0 \quad (1)$$

Also, the momentum equations reduce to the Bernoulli's equation

$$\frac{\partial\phi}{\partial t} + \frac{p}{\rho} + \frac{1}{2}\nabla\phi \cdot \nabla\phi + gz = C(t) \quad (2)$$

where  $p$  is the dynamic pressure,  $\rho$  is the fluid density and  $g$  is the gravitational acceleration. The function  $C(t)$  is the Bernoulli term and is constant for steady flows. On the free surface, the normal velocity of a point on the wave surface should be equal to the normal velocity of a fluid particle at that point. This kinematics' free surface boundary condition can be expressed as

$$\frac{\partial\eta}{\partial t} + \frac{\partial\phi}{\partial x} \frac{\partial\eta}{\partial x} + \frac{\partial\phi}{\partial y} \frac{\partial\eta}{\partial y} = \frac{\partial\phi}{\partial z} \quad (3)$$

where  $\eta$  is the wave elevation. For the inviscid fluid, the dynamic free surface condition requires that the normal pressure on the free surface be equal to the atmospheric pressure. When both the viscosity and surface tension are neglected, the dynamic condition on the exact free surface can be written as

$$\frac{\partial \phi}{\partial t} + \frac{1}{2} \nabla \phi \cdot \nabla \phi + \frac{\eta}{Fr^2} = 0 \quad \text{on } z = \eta \quad (4)$$

where  $Fr$  is the Froude number  $U_o / \sqrt{gL}$  based on a reference velocity  $U_o$ , a reference length  $L$ , and the gravitational acceleration  $g$ .

On the wetted body surface, the normal velocity of a point on the body must be equal to the normal velocity of the adjacent fluid,

$$\vec{V} \cdot \vec{n} = \vec{V}_s \cdot \vec{n} \quad (5)$$

where  $\vec{V}$  and  $\vec{V}_s$  are the fluid and body velocities, respectively,  $\vec{n}$  is the unit normal of the body surface. The same Neumann boundary conditions have also been used for the bottom and side wall boundaries. On the upstream boundary, the velocity potential for the incident wave is specified:

$$\phi = \sum_{n=1}^{\infty} \frac{gA_n \cosh k_n (h+z)}{\omega_n \cosh k_n h} \sin[k_n (x \cos \theta_n + y \sin \theta_n) - \omega_n t + \varepsilon_n] \quad (6)$$

where  $A_n$  is the wave amplitude,  $h$  is the water depth,  $k_n$  is the wave number,  $\omega_n$  is the wave frequency,  $\theta_n$  is the wave heading, and  $\varepsilon_n$  is the phase shift. In the far field, a radiation condition or absorbing beach must be employed to avoid wave reflections from the downstream boundary. Open boundaries enclosing the fluid domain are artificial and essentially arbitrary. In the present study, an absorbing beach proposed by Clement (1996) was implemented by adding a viscous term in the dynamic free surface boundary condition:

$$\frac{\partial \phi}{\partial t} = -\frac{1}{2} \nabla \phi \cdot \nabla \phi - \frac{\eta}{Fr^2} - v(x) \frac{\partial \phi}{\partial n} \quad (7)$$

The performance of the damping beach depends on the ratio of the beach length to the wavelength. A longer beach should be used for the shallow-water waves in order to reduce wave reflection from the end of the tank. The damping function employed in the present study is defined as

$$\begin{cases} v(x) = \beta \left( 1 - \cos \frac{\pi |x-x_1|}{|x_2-x_1|} \right) & x_1 \leq x \leq x_2 \\ v(x) = 2\beta & x_2 \leq x \leq x_d \end{cases} \quad (8)$$

where  $x_l$  and  $x_d$  denotes the beginning and ending locations of the damping beach. The coefficient  $\beta$  is chosen to be 0.1 for optimum performance of the damping beach.

In the present chimera Laplace method, the solution domain is first decomposed into a number of computational blocks. The body-fitted numerical grids for different parts of the geometry are generated separately. Within each computational block, the finite-analytic method of Chen, Patel, and Ju (1990) was employed to solve the Laplace equation for velocity potential on a general curvilinear, body-fitted coordinate system. The free surface boundary conditions were solved using a fifth-order Runge-Kutta-Fehlberg method to provide stable and accurate time-integration for wave-body interaction problems considered here. A more detailed description of the present numerical method is given in Chen and Lin (1998, 2000) and Kang, Chen and Huang (1998).

## MODEL SETUP

### **Basin and structure layouts.**

The 5T Basin is basically of rectangular shape with a rectangular cutout at the northeastern corner and a narrow indent at the eastern end of the south bulkhead. The south bulkhead is mostly vertical except the indent, while other bulkheads around the basin present a short ramp of roughly 30 feet wide. The basin is measured nominally 520 feet wide in the north-south direction and 670 feet long in the east-west direction up to the existing (north) breakwater. Its long axis lays roughly 15 degrees south of the due west. The existing breakwater runs about 240 feet from the western end of the north bulkhead toward the south, leaving a basin entrance of roughly 280 feet wide at the west border. The south bulkhead extends 284 feet further west of this breakwater. An L-shaped fuel pier and four floating docks spread along the north bulkhead and a major pile supported pier (5T Pier) runs along the western half of the south bulkhead near the basin entrance. Water depth inside the basin varies drastically from 40 feet at the entrance to less than 10 feet in the area of floating docks along the north border.

Key dimensions of basin geometries and locations of pier facilities were extracted from a sketch of basin overall plan (Figure 4) and enhanced with measurements from a sketch of breakwater layouts (Figure 2). Both are furnished by the sponsor. The results were further refined in accordance to field measurements<sup>5</sup> as illustrated in Figure 5a. Dimensions of the floating docks and fueling pier were adopted from a floating dock system calculation report<sup>6</sup>. These facilities were treated as fixed floats at a draft of 30 inches throughout the analysis. Their dynamic responses can be addressed with the same model by activating the motion tracking modules in the code as described by Huang and Chen (2003). The 5T Pier is a pile supported structure with its entire deck clear of the

---

<sup>5</sup> Conducted by Mr. Dennis Clark and Mr. Richard Kahler of NAVFAC Atlantic.

<sup>6</sup> Floating Dock System Calculation Report at Navy Small Boat Basin, Norfolk, VA. Prepared by Carter & Sloope Consulting Engineers, June 26, 2003.

water surface and was thus not shown in the numerical model. Figure 5b summarizes the basin geometries and structure layouts implemented in the numerical model. The south breakwater was implemented at the proposed location as shown in Figure 2. Its length and orientation are adjustable. In order to facilitate time-domain simulations of wave transformation involving complex coastal features, a separate wavemaker grid was used for concurrent computation of the incident wave field in the absence of the structures. An absorbing beach was placed in front of the wavemaker to eliminate the wave reflections and diffractions from the structures and/or the irregular harbor shorelines. This maintains the incident waves at a constant intensity over an extensive simulation duration. The dimensions of the wavemaker grid vary with the length and heading of incident waves. This will be discussed in more detail later.

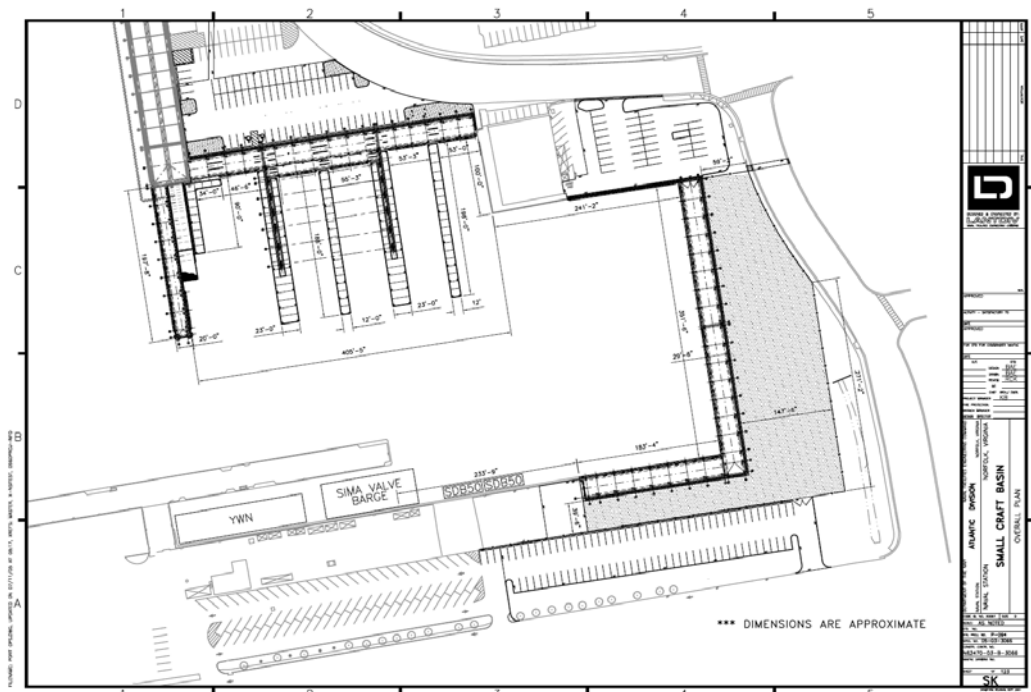


Figure 4. Sketch of overall plan of 5T Basin.

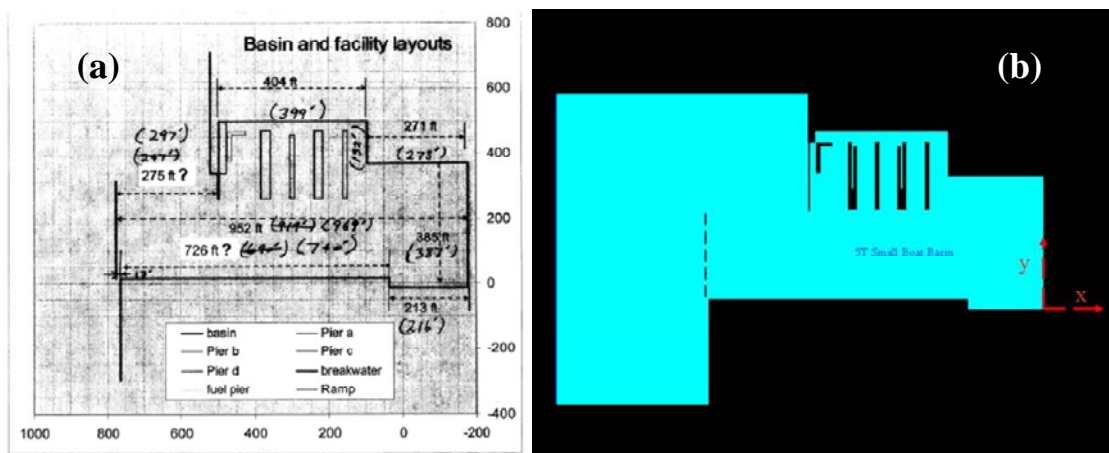


Figure 5. (a) Field confirmations of basin geometry, (b) numerical representations.

## Numerical Basin.

**Sea bed.** The sea bed geometry was reconstructed from a sponsor supplied echo sounding chart as shown in Figure 6. However, measurements near 5T Pier and floating docks are scarce on this chart. The missing data were patched with the best estimates by field engineers. Sea bed beyond the echo sounding chart was represented by a mesh at a constant depth of 45 feet, which subsequently faired into the charted sea bed at the overlaps. A continuous surface attaching to these discrete nodes was generated by linear interpolation. The result is presented in Figure 7a. This surface provides a database for grid generation at the sea bottom. Figure 7b is a close-up view near the floating docks and fueling pier. Several key profiles of the sea bed were summarized in Figure 7c. It can be seen that the basin can be roughly divided into three zones by depths. Zone A at the southwestern corner was dredged to a rectangular depression of 38-feet deep surrounded by sheer slopes. This zone extends from the present basin entrance to roughly the mid basin. The sea bed beyond this depression (Zone C) rises sharply to flat beds of roughly 20-foot deep across the east basin before tapering to the free surface within the last 30 feet from the east bulkhead. Zone B to the north of the depression rises gradually to 10 feet in the area around the floating docks. Water depths along the south bulkhead are relatively deep with water depths vary from 40 feet around 5T Pier and gradually taper to 10 feet near the east bulkhead.

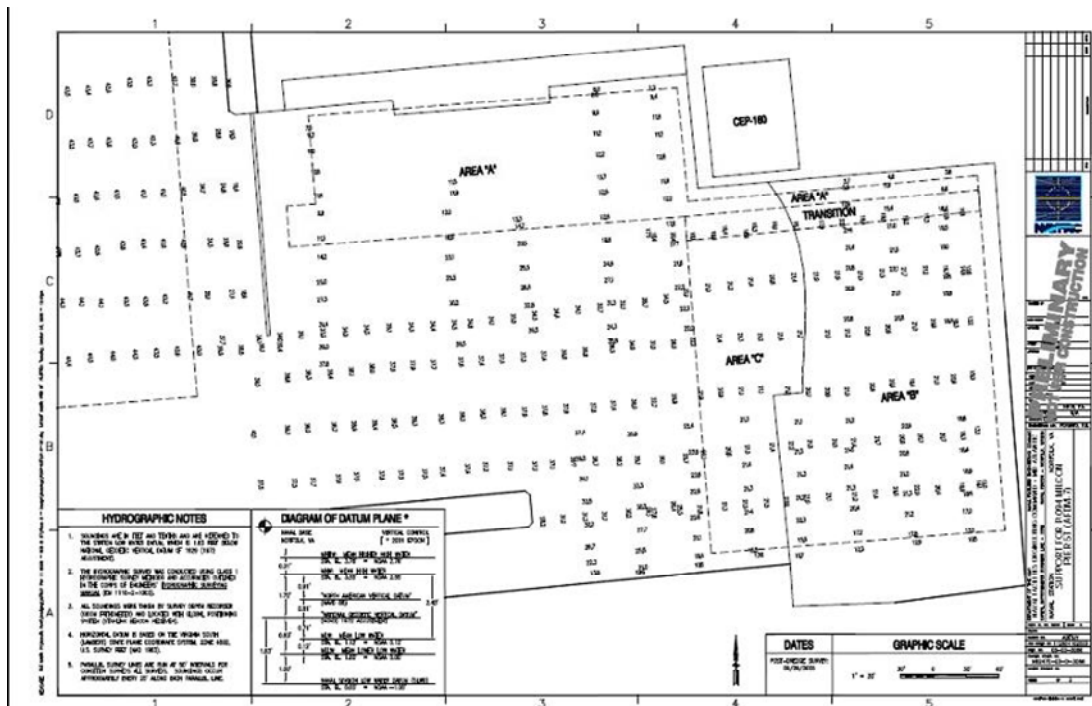


Figure 6. Echo sounding chart of 5T Basin.



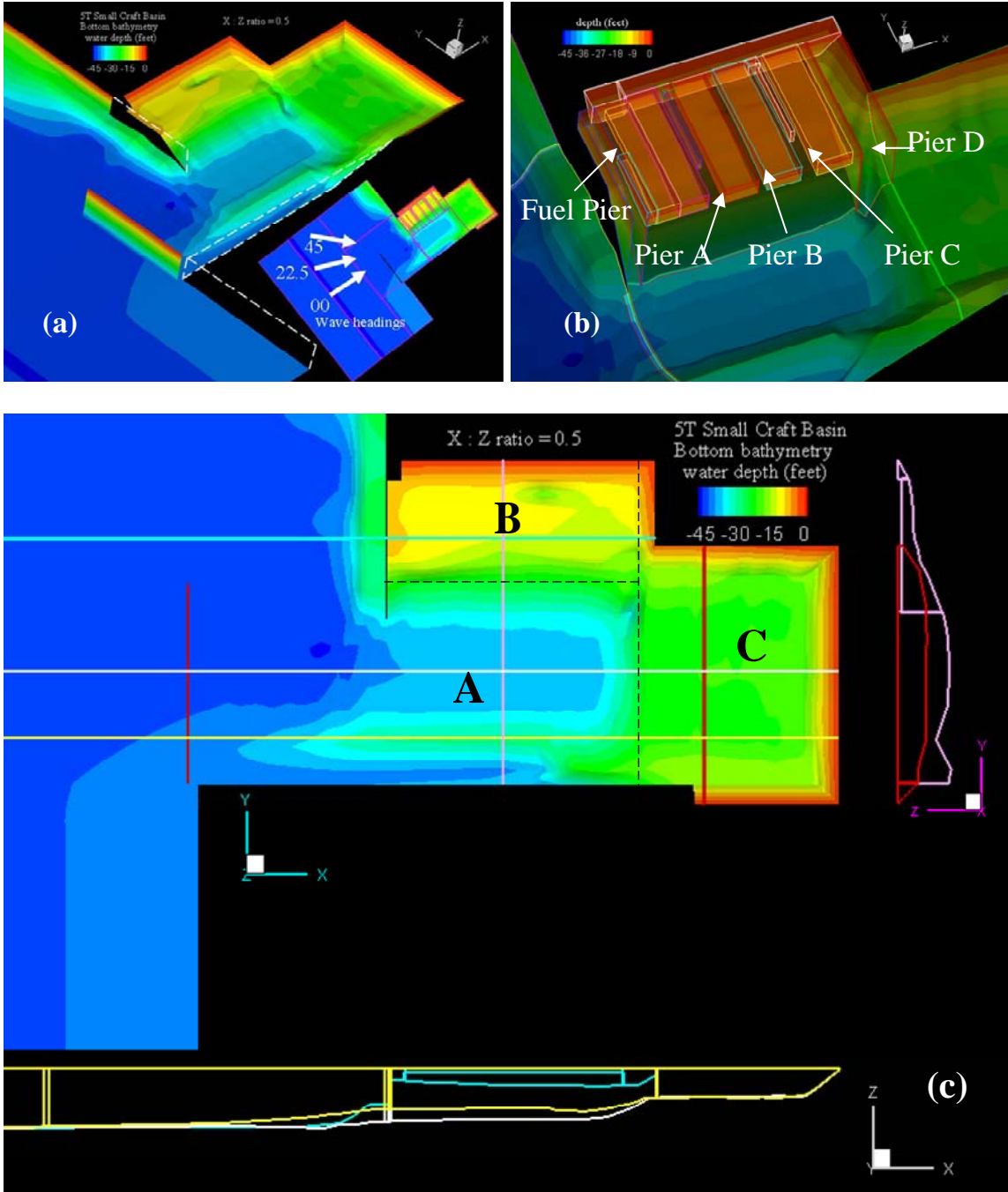


Figure 7. (a) Sea bed bathymetry, (b) floating docks, and (c) sea bed profiles.

**Grid System.** The fluid domain was divided into multiple blocks of simple geometries for the convenience of grid generation. A total of 25 grid blocks were used to cover the solution domain. Figure 8a illustrates the layouts of background blocks for the case of 4-second waves approaching from 0 degree. The blocks inside the present basin area and three blocks immediately outside the north breakwater are referred as basin blocks. They are used to describe the basin and coastal structures (Figure 8b). The rectangular block at the upstream most edge enclosed in red boundaries represents a wavemaker. This block is connected to the basin blocks through a transition block enclosed in blue boundaries.



These two slender rectangular blocks constitute a wave tank where incident waves evolve and propagate before entering the basin blocks. The block enclosed in green boundaries, which overlaps the entire wavemaker block and a part of the transition block, is a stand-alone numerical wave tank with its own damping beach at the downstream end. This block never links with any block. Its sole purpose is to provide a reference of unpolluted incident wave array. This reference is used in conjunction with the waves in the tank blocks to identify the reflection waves in such blocks arriving from the coastal structures downstream. An absorbing beach in the wavemaker block subsequently dissipates the reflection waves before they reach the wavemaker, and as such maintain the quality of incident waves for extended simulation durations. Each of these 25 blocks are digitized into a three dimensional grid separately as illustrated in [Figure 8c](#).

[Figure 7b](#) provides a close up view of water domains around the five floating piers. A series of small grid blocks surrounding the floating piers represent a layer of water at the same elevation. The piers occupy the voids in between. These blocks in turns overlay a background block covering the general area of floating docks. This illustrates a typical application of the chimera decomposition technique in congested water domains around irregular solid boundaries. This arrangement allows the small blocks be digitized individually to resolve local details. Most grid blocks are essentially “hard-wired” to their adjacent blocks to keep the size of numerical model manageable. Any change in these blocks will require manual attention. The O-type breakwater grid is the only exception. This block is completely embedded in the basin grid and can be easily rescaled or relocated without regenerating the basin grid. A utility routine in the present code automatically searches interpolation correlation across the block boundaries in case the breakwater is reconfigured in size, shape, or orientation. This simplifies the grid generation process for parametric studies of various breakwater configurations. The benefit is achieved at the cost of committing a greater number of grid nodes however.

The chimera technique allows each block to be digitized individually into a three dimensional grid system. The grid sizes in use must be sufficiently fine to preserve: (a) the details of basin geometries, (b) the shapes of piers and breakwaters, and (c) the shortest waves in consideration. It is preferable to place at least 4 nodes on any edge of a structure and 20 nodes in each wavelength. For the present study, the grid sizes inside the 5T Basin are dictated by the shortest wavelength and the smallest structure dimension. Considering couplings among incident, reflection and diffraction waves, all grids inside the basin or in contact with breakwaters or bulkheads were digitized to fine resolutions of 1 to 4 feet. The grids on the free surface and the four vertical sides of a block may be generated with ample flexibilities. However, the bottom face must precisely attach to the sea bed. This was accomplished by mapping the surface grids onto the sea bed database prepared in the previous section.

It is desirable to reserve at least three wave lengths for the wave tank blocks to ensure their functions. An 8-second wave is roughly four times as long as a 4-second wave in deep water. Therefore, the required size of the wave basin varies drastically. Fortunately, longer waves tolerate larger grid sizes providing the premise of 20 nodes per wave length is honored. It is necessary to refine the wave tank model for each individual

case to maintain a proper grid resolution and to keep the model size within the limitations of the current FORTRAN compiler for PC workstation applications. Consequently, a total of five distinct numerical models were generated for incident waves of 4, 6, and 8 seconds approaching from 0 degrees (Figure 9a) and incident waves of 4 seconds approaching from 22.5 and 45 degrees north of the long axis of the 5T Basin (Figure 9b), respectively. Each was customized to preserve the overall accuracy and computation efficiency.

Damping beaches were also implemented along the lateral domain boundaries, with very coarse grids just enough to prevent the outgoing waves from reflecting back to the analysis domains. Due to the significant velocity and pressure gradients along the water column, a total of 11 grid layers were used in the vertical direction with a maximum grid size of 4 feet. The total number of grid points including the absorbing beach is about 1.81 million.

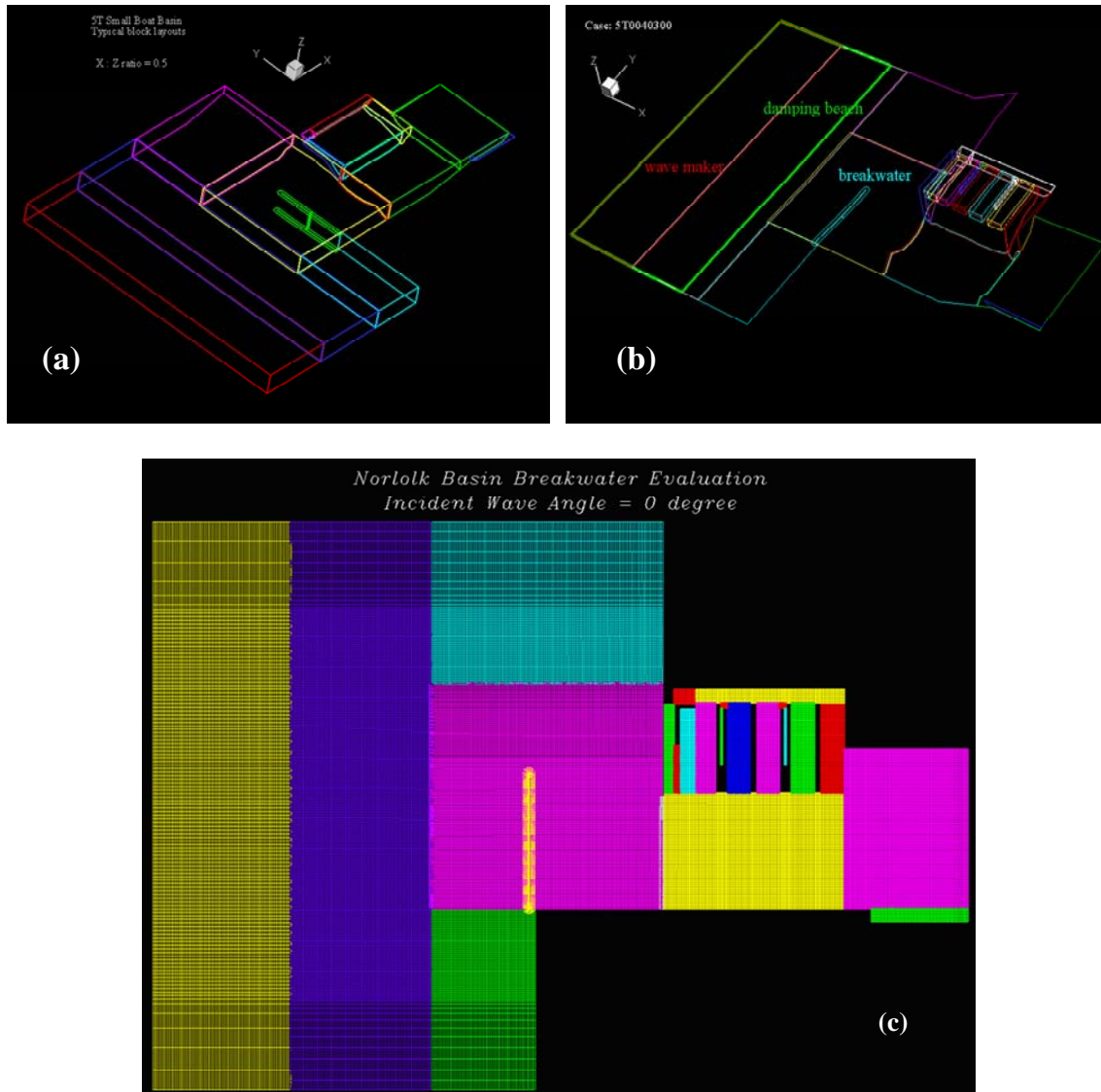


Figure 8. (a) block layouts, (b) wave maker, and (c) grid systems.

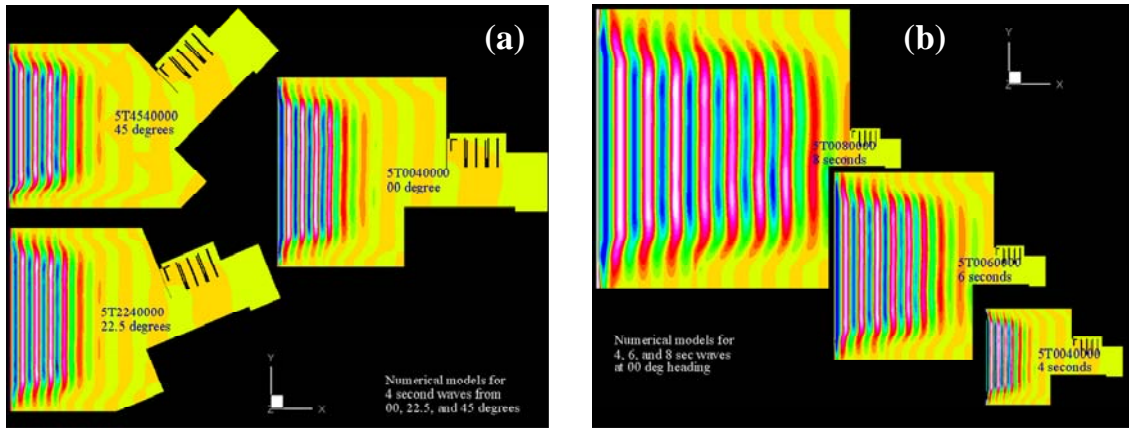


Figure 9. (a) models for various wave headings and (b) periods.

**Incident waves.** The maximum daily recurrent wind waves at the target site are likely of low Sea State 3 with a mean period around 4 seconds given the storm duration and limited fetch of the inland water at Hampton Roads. Field observations indicate that these waves often approach within 45 degrees of due west. Waves from directions outside this sector are sheltered either by land mass or moored ships along the waterfront and thus present little threat to the 5T Basin. Consequently, this study considers primarily 4-second waves from 0, 22.5, and 45 degrees north of the long axis of the 5T Basin as shown in Figure 9a. Two additional waves of 6 and 8 seconds (Figure 9b) are used to explore the sensitivity of basin responses to longer waves.

The incident waves are generated by a wavemaker installed at the upstream edge of the numerical wave tank. Although this wavemaker is capable of generating a wide range of irregular waves, this study proceeds with regular (or monochromatic) waves of unit amplitude for easier tracking of the anticipated busy wave patterns inside a confined water over complicated sea bed like the present site. The wavemaker was instructed to generate wave arrays of prescribed lengths. Figure 10 illustrates incident waves of 80-, 160-, and 320-feet long before the energy fronts reaching main bulkheads. The corresponding wave periods are roughly 4, 6, and 8 seconds. All profiles are drawn from an identical cross section through the basin entrance. Note that the proposed south breakwater has yet to be installed in this case. It can be seen that the wave array quickly reaches the target intensity of unit amplitude and maintains steady in length and height. Several typical features of a progressive wave are also observed. For instance, the longer waves travel faster than the shorter ones in deeper water as anticipated. The clear energy front leading each wave array further substantiates the quality of incident waves produced by the present wavemaker. The shape of the wave front for the 4-second waves (yellow line) is almost identical to prediction by linear theory (red dots).

Figure 11 illustrates the incident waves of 4 seconds approaching from a 0-degree heading at five selected time instants with the presence of the south breakwater. In this figure,  $t$  and  $T$  indicate the elapse time and wave period, respectively. The wave heights are scalable. The free surface elevation along a constant- $y$  line across the south breakwater is also shown in the lower right corner of each figure. The simulations were performed for 5,000 time steps at a time step increment of  $0.0125 T$  (i.e., 80 time steps

per period). Note that the wave profiles are color coded by grid blocks. The green section on the weather side of the south breakwater illustrates actual wave activities resulting from significant couplings of incident waves with reflections by the breakwater. The reflected waves, which are supposed to propagate up to the wavemaker in reality, were gradually dissipated over the damping beach (the yellow section) in front of the wavemaker block. The incident wave profiles (the red section) are hence free from the influence of reflected waves and remain steady throughout the simulation duration. This wave component continues to propagate through the damping beach into the basin blocks.

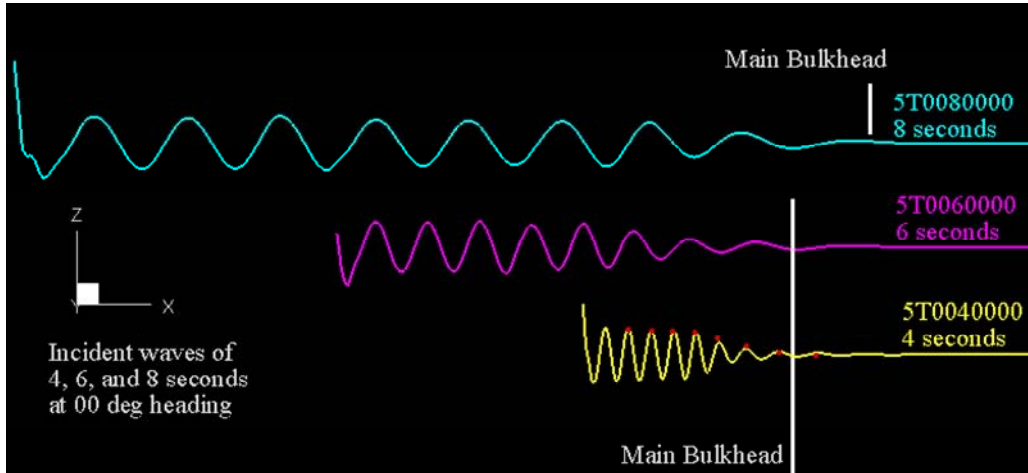
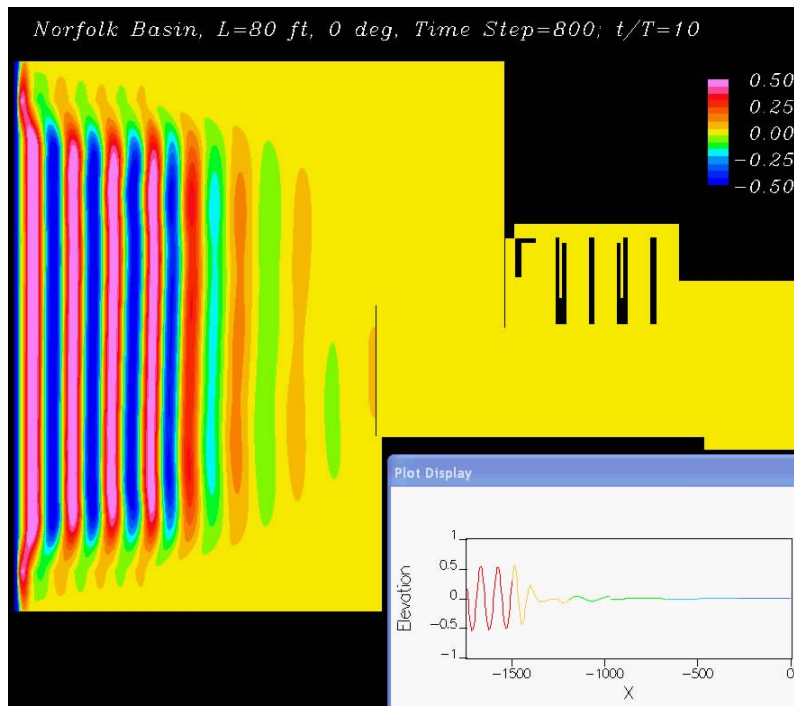


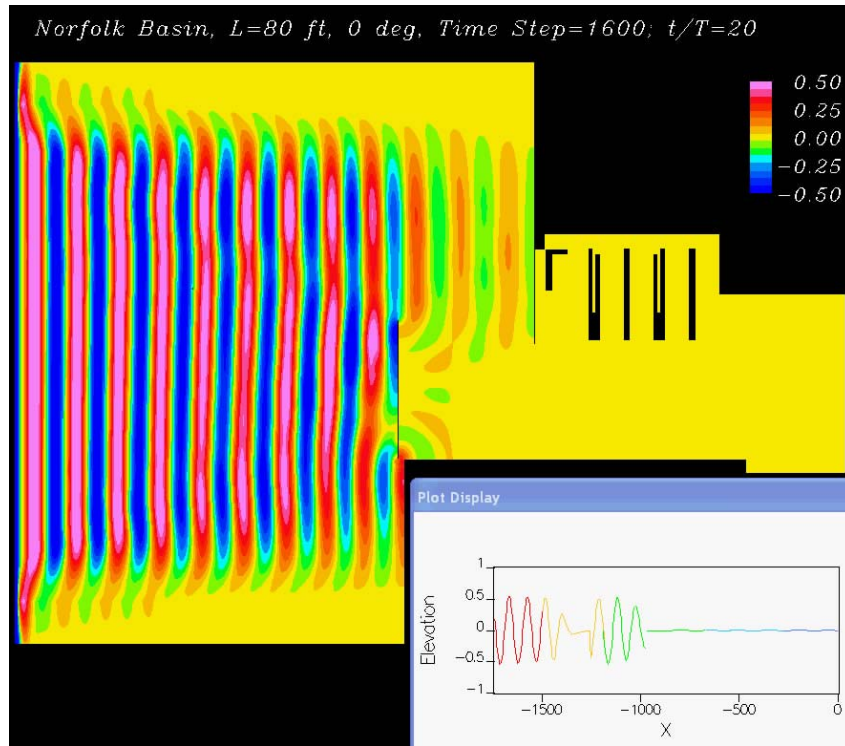
Figure 10. Incident waves of 4, 6, and 8 seconds.



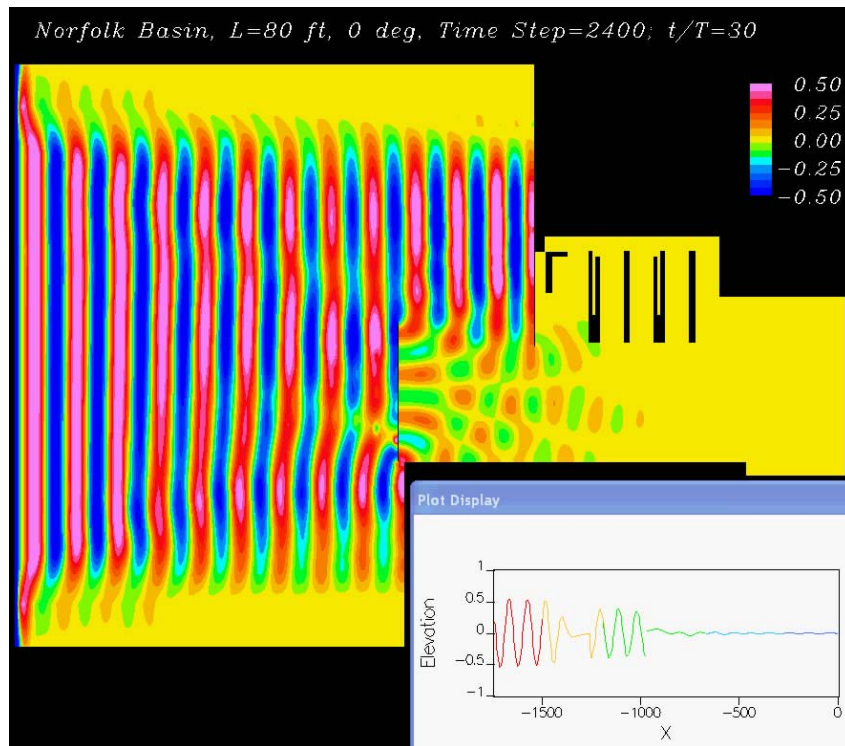
(a)  $t/T = 10$

Figure 11. Example of incident waves of 4 seconds from  $0^\circ$  heading.



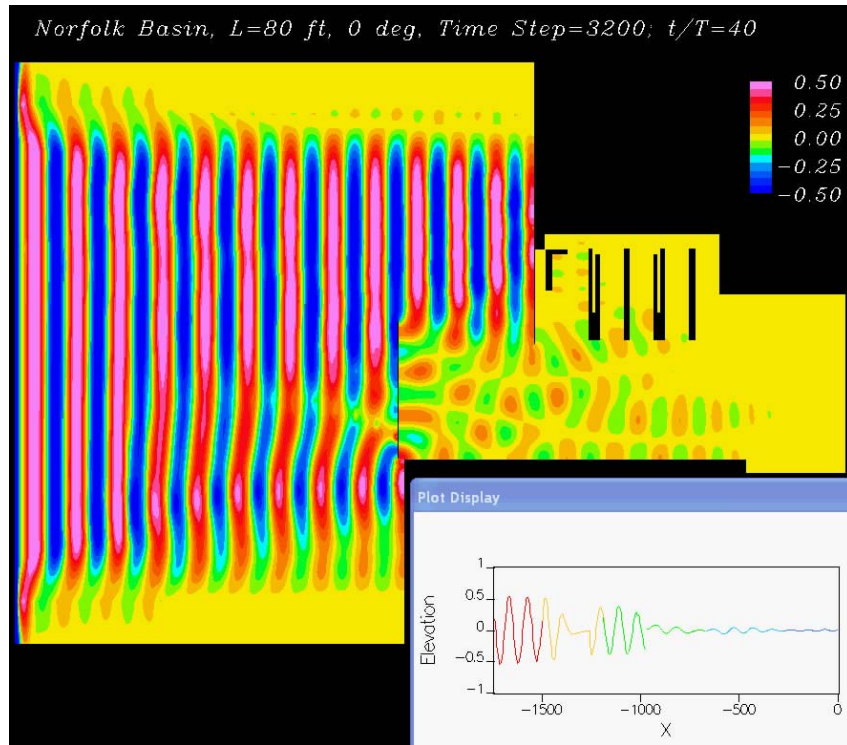


(b)  $t/T = 20$

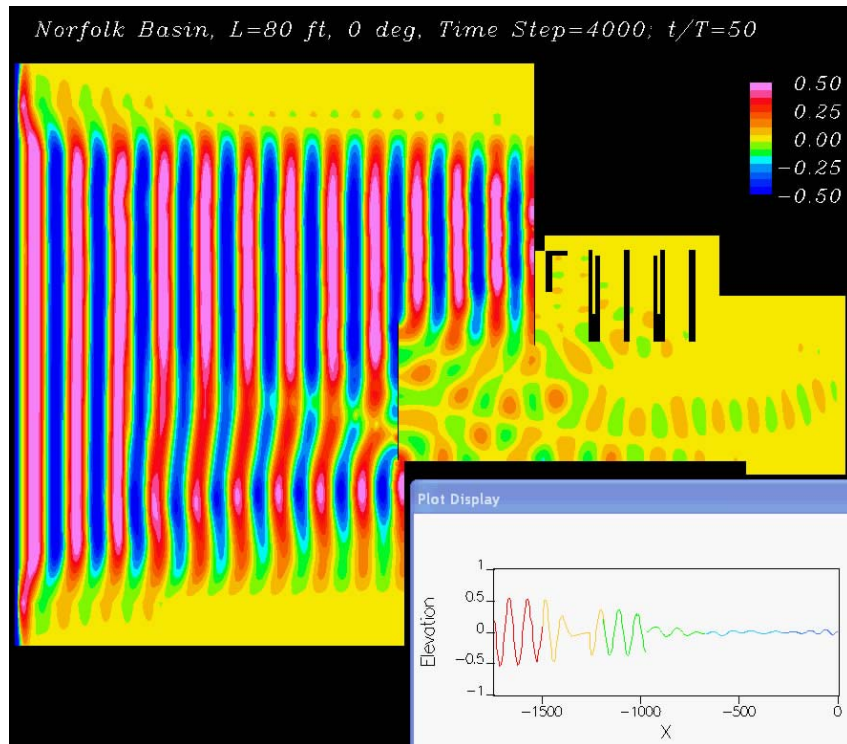


(c)  $t/T = 30$

Figure 11. Continued.



(d)  $t/T = 40$



(e)  $t/T = 50$

Figure 11. Continued.

## RESULTS

Two series of simulations were conducted to observe wave fields at the 5T Basin before and after the installation of the south breakwater. The contrast between these two series delineates the performance of this breakwater. For convenience, the wave fields are described in terms of wave transmission coefficients,  $K$ , or the ratio in percentages of the local wave height ( $H$ ) to the incident wave height at the wavemaker ( $H_i$ ).

### **Wave activities without the south breakwater.**

The first series explored the wave fields without the south breakwater induced by local wind waves of 4, 6, and 8 seconds. The results provide a sanity check of the hydrodynamic nature of this basin as is and set a tangible base for evaluating the effects attributable to the south breakwater. This series of simulations were performed for a total of 62.5 wave cycles, or simulation durations of 250, 500, and 1000 seconds for 4-, 6-, and 8-second waves, respectively. Therefore, the predicted wave activities are likely to occur in most storms. It seems reasonable to adopt incident waves associated to 1-hour sustained winds for simulations.

[Figure 12](#) is a snap shot of wave activities inside the basin at an instant near the end of the 56<sup>th</sup> cycle. Colors indicate the free surface elevation in terms of transmission coefficients. For clearness, their values at selected highs and lows are also shown. Keep in mind that the waves inside this irregular basin are highly dynamic, as such, extremes of the free surface at all locations do not occur concurrently. The embedded movie clip next to the image provides a complete history of the resulting wave activities. In addition, the free surface profiles along three constant- $y$  lines are also shown below the image. These profiles are color coded in compliance with their respective location lines shown in the image. Nevertheless, this image gives a concise overview of the entire wave field and identifies critical spots of high intensities.

Waves inside the basin are indeed substantial and complex. Recall that this basin consists of three rectangular zones of distinct water depths ([Figure 7c](#)). Zone A was dredged to roughly 38 feet deep and measured 300 feet wide by 400 feet long. Zone B and Zone C are elevated to flat beds of roughly 10 and 20 feet deep, respectively. It can be seen from the movie clip that the ambient waves enter primarily through the depression while a lesser amount diffracts around the north breakwater and subsequently radiate into the surrounding shallow basin. Waves in the shallow zones are mild initially. However, they grow in time to a respectable size of 20% or higher as the trailing waves continue to saturate the basin in about 50 wave cycles. At this moment, the wave heights in the depression are about 50% of the incident wave height and may reach 95% at certain spots along the south bulkhead as depicted by [Figure 12](#). The trapped waves bounce around the basin and eventually trigger various low-frequency oscillations. A closer review of the embedded movie clip further reveals clear signs of partial standing wave patterns in front of the breakwater and the east bulkhead of the basin.



The overall wave pattern inside the 5T Basin somewhat resembles the theoretical diffraction diagram (Figure 13) provided by Johnson (1952)<sup>7</sup> for a comparable shoreline consisting of an unbounded straight barrier with a gap in the middle in open water of constant finite depth. Since this layout was perfectly symmetrical, the line of symmetry can be treated as a solid boundary equivalent to the south bulkhead of 5T Basin. This basin fits roughly in the area enclosed by the red box. One-half of the gap width is 2.5 wave lengths, which is close to the width of the entrance of 5T Basin normalized by the length of 4-second waves. It can be seen from Figures 12 and 13 that the wave patterns along the geometric shadow line of the north breakwater and the south bulkhead in both cases are essentially the same and reasonably close to their respective theoretical value of 0.5 and 1.0. The wave patterns behind the breakwater are also comparable. Nevertheless, substantial disparities exist elsewhere, especially at the shallow waters and vicinities of peripheral bulkheads. This result implies that wave activities in the basin are dictated by diffractions but substantially modified by radiations and refractions. Shoaling effect is minor for good reasons. The actual water depths of the basin vary from 50% to 5% of the wave lengths in consideration. Linear theory (e.g., Wiegel, 1948)<sup>8</sup> indicates that waves in this range tend to decrease slightly by no more than 10%. Besides, the tight space and rapidly changing sea bed may not allow full evolution of shoaling at all. For instance, the immersed sheer banks around the deep depression are more likely to reflect wave energy than to alter the wave profiles. There is evidence that only the portion of wave energy above the slope transmits into the shallow water behind this depression.

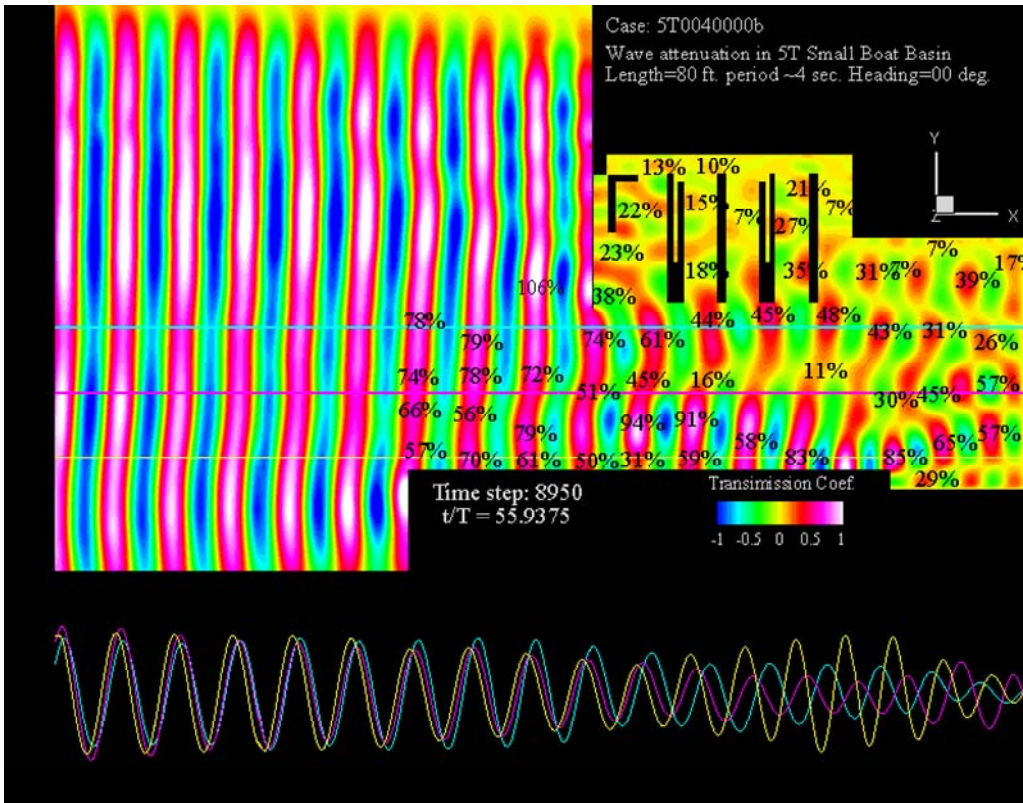
Wave activities inside 5T Basin is much more complex than predictions by the theoretical diagram. The tangled wave pattern is an apparent consequence of constant wave reflections off the peripheral bulkheads. Yet, much of the free surface complexities should be attributed to standing waves (Figure 14) and cross basin oscillations (Figure 15) underlying the surface waves. Both features are common in a confined basin even with a perfectly flat sea bed. These induced features are automatically addressed in the present method. Similar attempts with the traditional analytical models will be extremely labor intensive.

Figures 16 and 17 summarize the results induced by oblique waves of 4 seconds approaching from 22.5 and 45 degrees off the long axis of the basin. These oblique waves obviously are more damaging to the basin. The south bulkhead reflects incident waves into the basin like a mirror (hdgo1L.avi). As a result, the wave heights are much higher over the entire basin than the consequences induced by the same waves from 0 degree heading. The transmission coefficients along the south bulkhead increase drastically as high as 145% in 22.5 degree waves and 160% in 45 degree waves. The intruding waves were guided into the north half of the basin covered by the north breakwater. Wave heights there are more than doubled. The cross basin oscillations are also much more pronounced. It can be seen from the movie clips that the mean elevations of the water surface oscillate substantially, especially near the south bulkhead. Besides, the reflected waves couple with the incident components and create extensive short-crest ring waves near the basin entrance. This may concern small boat operations.

---

<sup>7</sup> Excerpted from Shore Protection Manual, 1984, Page 2-98.

<sup>8</sup> See Shore Protection Manual, 1984, Appendix C, Plate C-1, Page C-2.



5T040c.avi  
 5T040c\_rfrca.  
 vi  
 5T040c3D\_a.a  
 vi

Figure 12. Wave distribution without south breakwater (prd= 4 sec, hdg=00 deg).

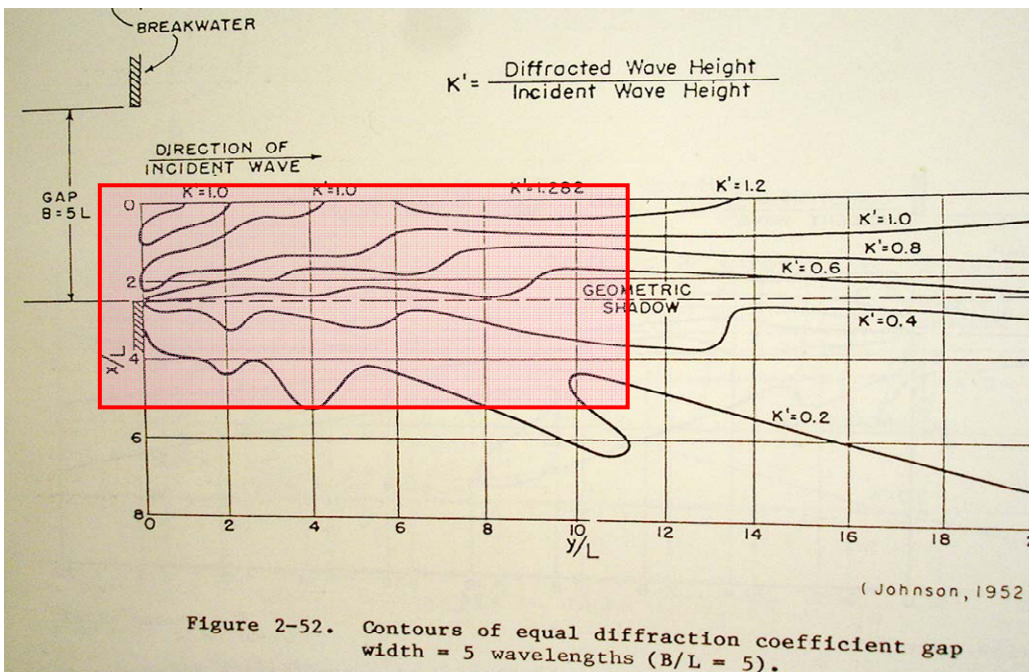
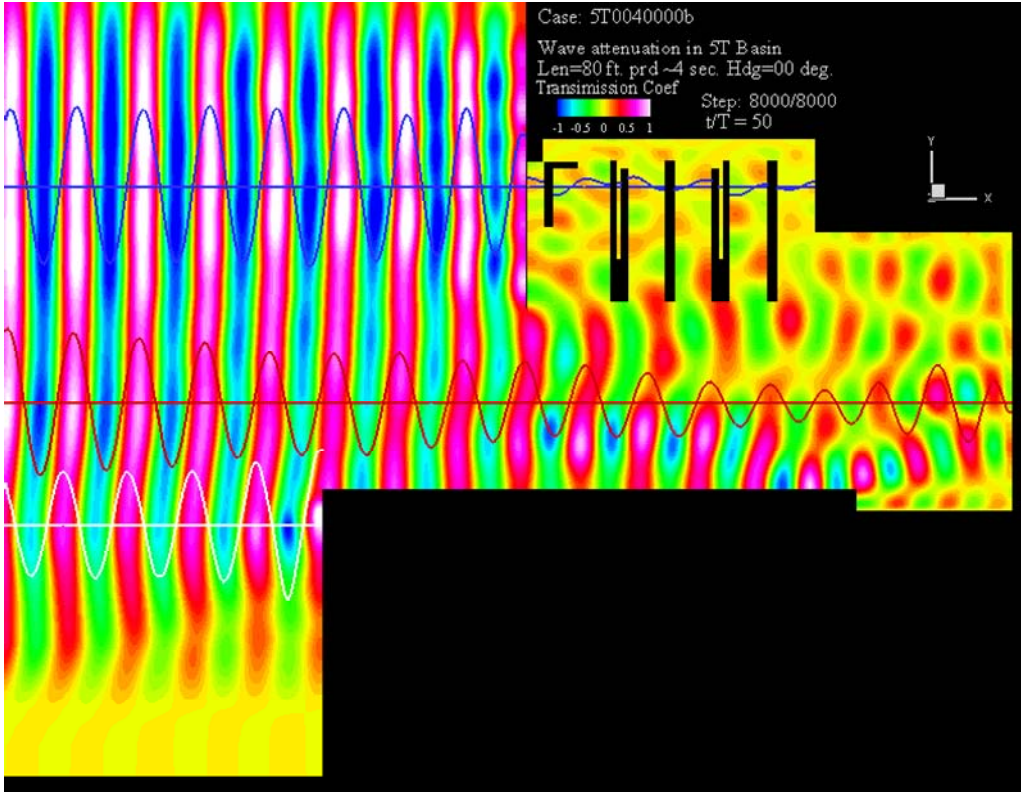
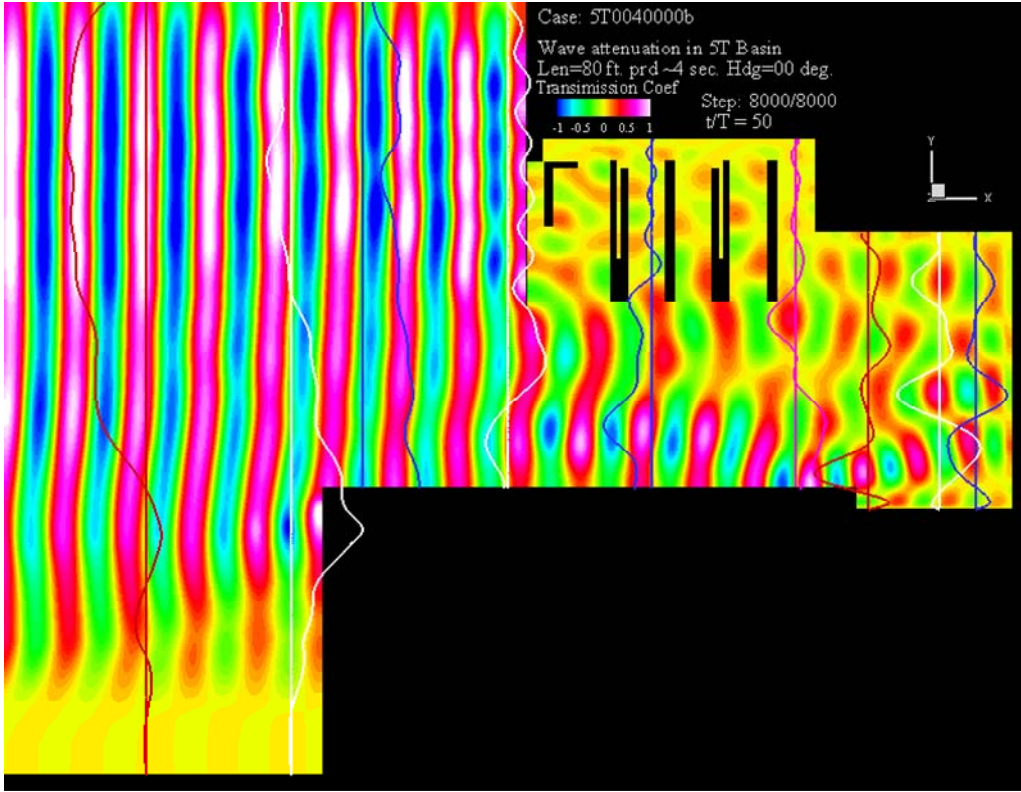


Figure 13. Diffraction pattern through a gap of five wave lengths, Johnson (1952).<sup>5</sup>



5T040bx.avi

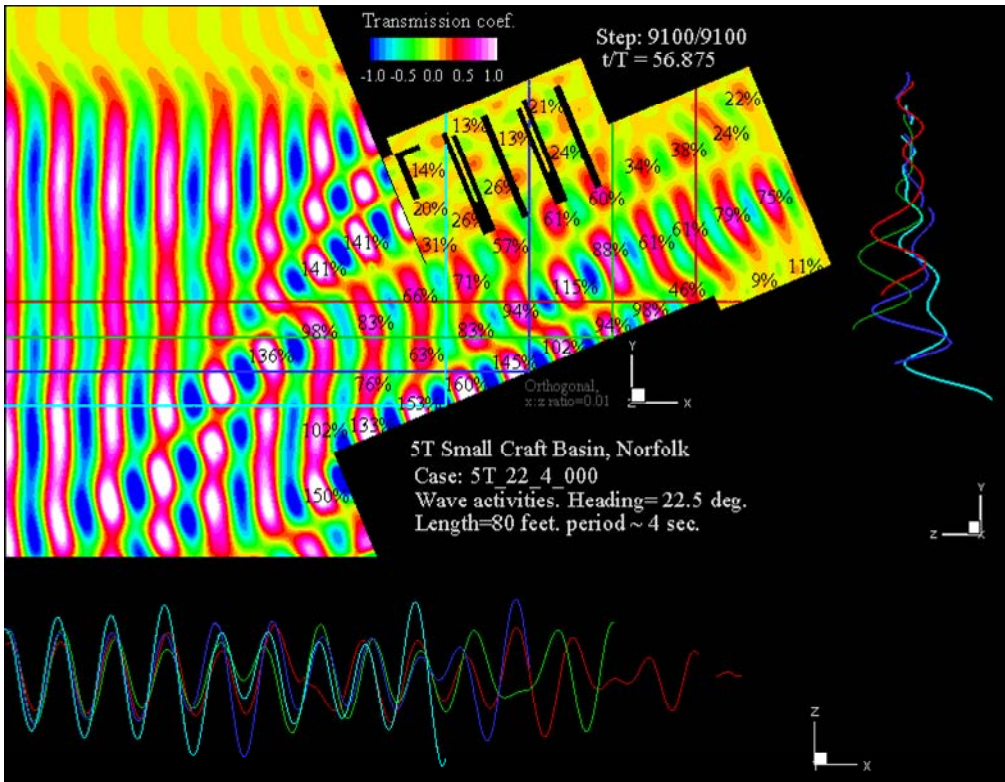
Figure 14.. Standing waves in front of bulkheads.



5T040by.avi

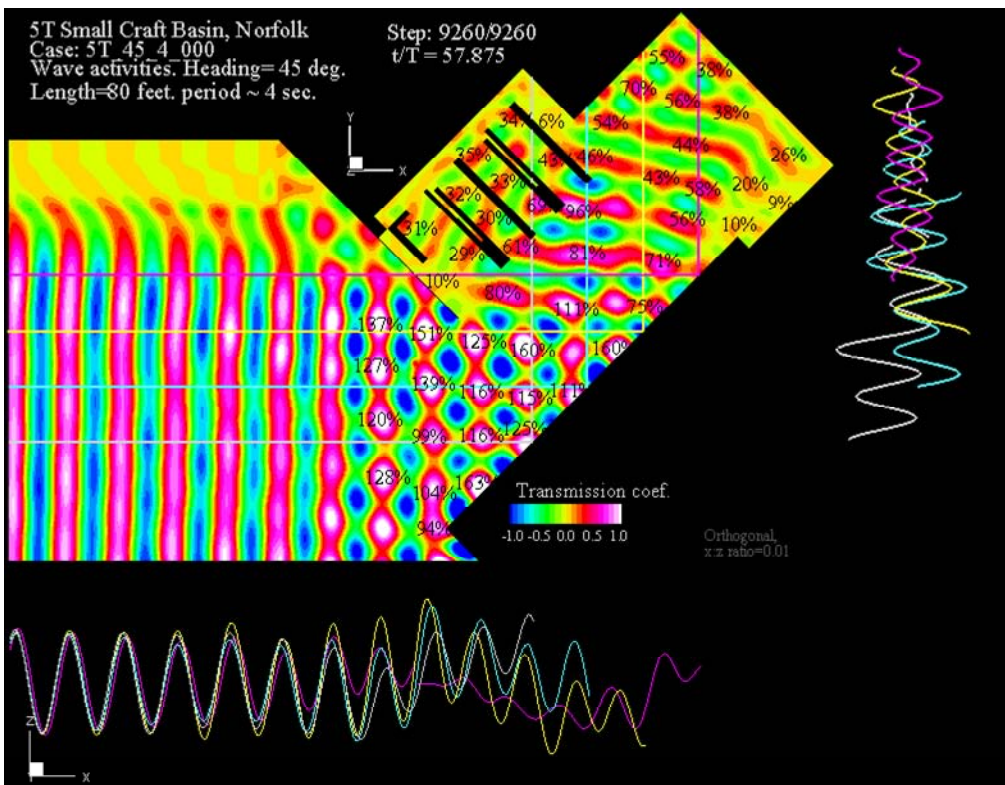
Figure 15. Cross Basin oscillations.





5T240.avi

Figure 16. Wave distribution without south breakwater (4 sec, 22.5 deg).

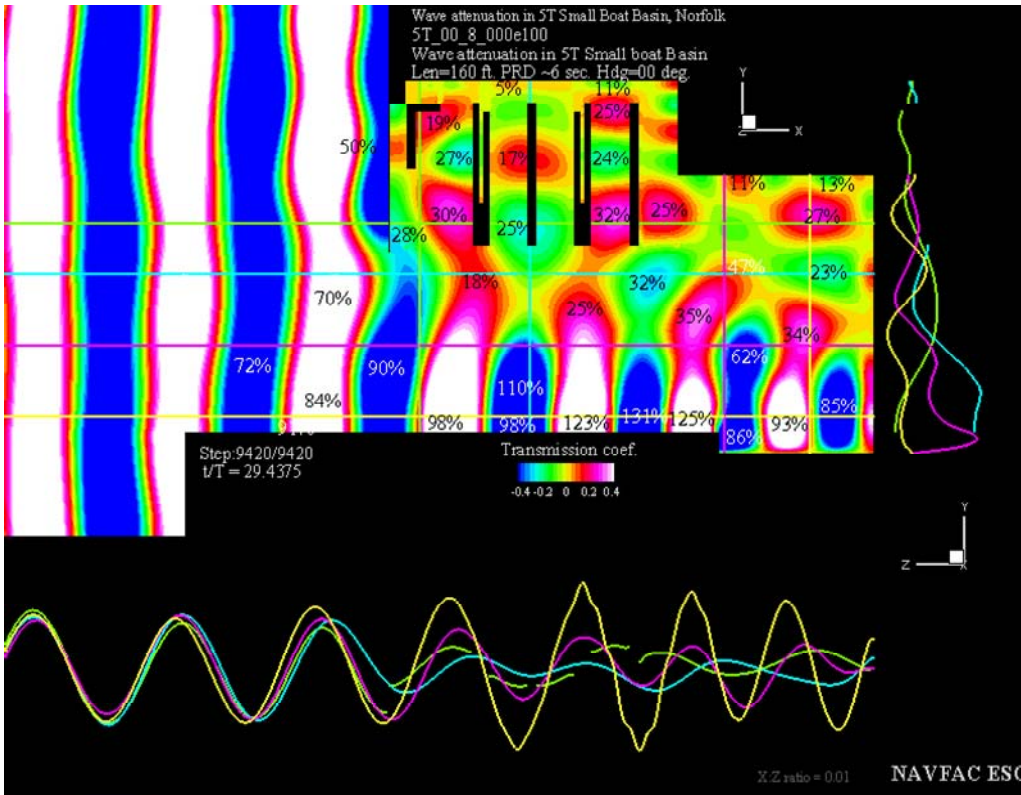


5T440.avi

Figure 17. Wave distribution without south breakwater (4 sec, 45 deg).

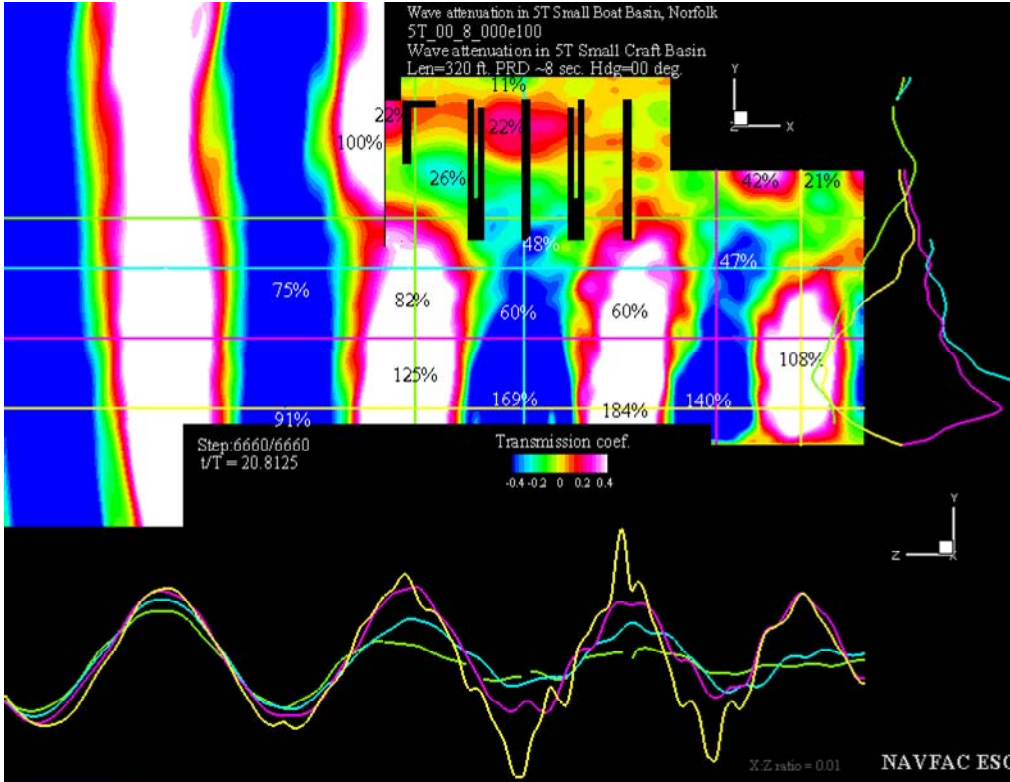
Figures 18 and 19 present the simulation results of 6- and 8-second waves to show the sensitivity of basin responses to wave lengths. The wave patterns look reasonable. In general, the longer waves penetrate the basin more effectively and result in higher wave disturbances. Basically, the basin size and its depth differentials reduce relative to wave lengths. In theory diffractions are anticipated to be farther reaching and refractions less obvious. Figure 20a properly reflects the general trend of higher waves and straighter wave crests over all for longer waves. The associated movie clip, [sum\\_prd\\_open.avi](#), further illustrates the evolution of standing waves next to the east bulkhead. One exception is the uncharacteristic high waves observed along the dash line in the case of 4-second waves. Waves along this line are substantially higher than their neighbors as illustrated in movie clip [5T040c\\_rfr.avi](#). The same is less noticeable in 6-second waves and nearly invisible in 8-second waves. This is actually in line with the sea bed geometry. As previously shown in Figure 7c, the sea bed presents a narrow ridge along this line near the south bulkhead. The shorter 4-second waves tend to converge toward the ridge line more pronouncedly than would the 6- and 8- second waves. This premise is further supported by the fact that similar humps of wave distributions are not observed in oblique seas. Taking away this refraction factor, the high transmission coefficients near the south bulkhead in Figure 12 would have been around 70%. Incidentally, the overall picture of wave transmission is more consistent with the theoretical anticipation that longer waves tend to penetrate a physical gap more effectively. A closer review of the associated movie clips reveals that standing waves at the east bulkhead are more pronounced and appear sooner in longer waves.

Note that the 8 second waves excite the basin much more intensively than the shorter waves do. Waves along the south bulkhead reach 184% of the incident heights. They also induce more pronounced standing waves in the east basin; perhaps the longer waves are less dispersive by nature. The waves shrink in length and seem to grow in height (considering dispersion effects) as they enter the shallower east basin. Wave heights there are comparable to the ambient seas. Similar trends, although less obvious due to stronger dispersions, were also observed with 4- and 6-second waves at late stages when the wave field was more saturated (Figure 20b). This usually implies shoaling effects. However, the profile of 4-second waves of the same figure also signals basin oscillations. Movie clip [5T080b.avi](#), which traces the wave history at time increments of one wave cycle, seems in favor of the latter observation. Evidences are insufficient to differentiate basin oscillations from shoaling effects for the time being. Additional tests with a flat sea bed in the basin are required to clarify this picture.



ST060a.avi  
 ST060b.avi  
 ST060.avi

Figure 18. Wave distributions without the south breakwater (6 sec. 00 deg).



ST080a.avi  
 ST080b.avi

Figure 19. Wave distributions without the south breakwater (8 sec. 00 deg).



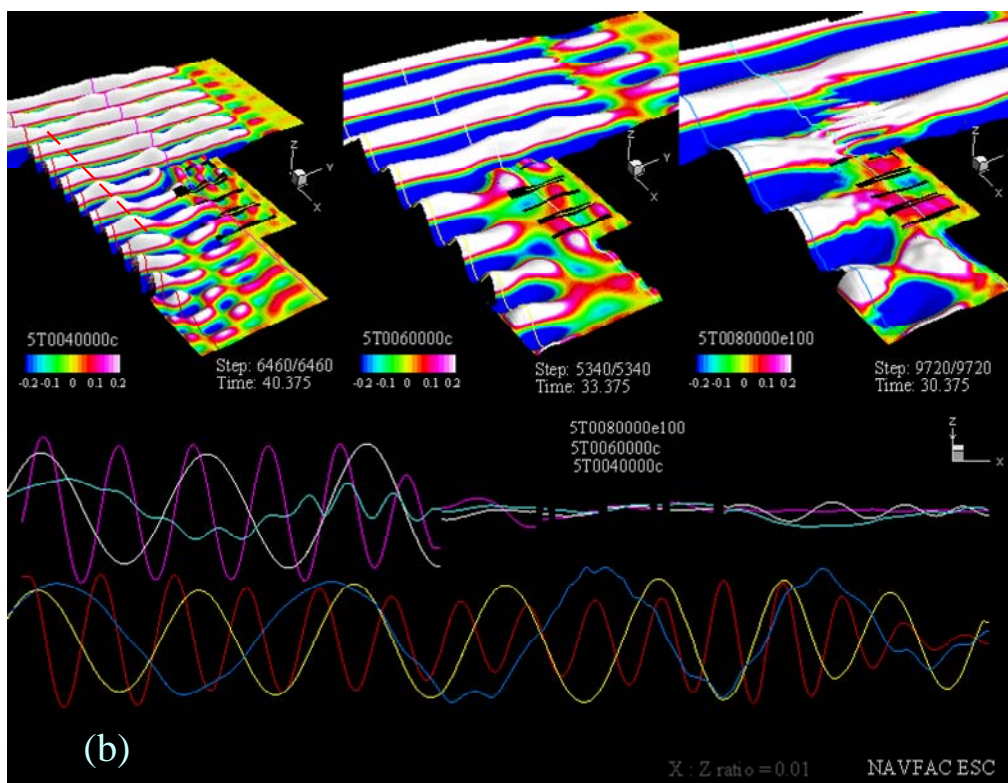
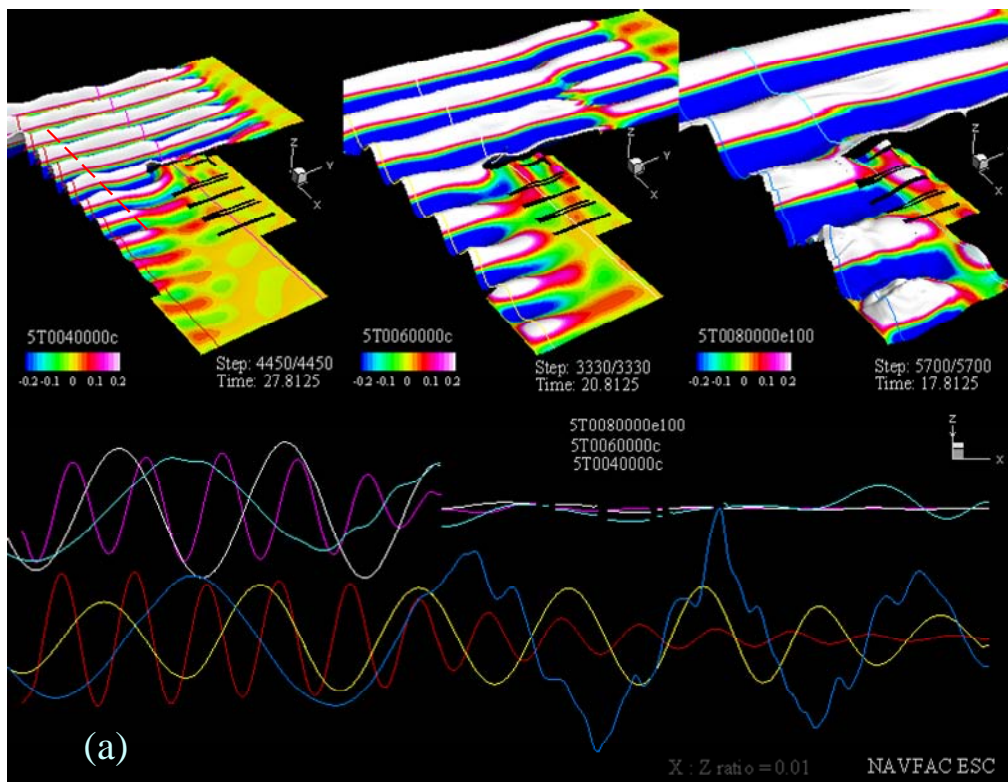


Figure 20. Sensitivity of wave lengths without the south breakwater



## **Wave activities with south breakwater.**

The second series revisited all cases of Series one after implementing the south breakwater. The numerical models remain the same as before except an additional block for the south breakwater. Incident waves are identical. The simulations with 4-second waves were performed for 10,000 time steps with a time increment of 0.00625 T (i.e., 160 time steps per period), or a total of 62.5 wave cycles. It was, however, necessary to reduce the time increment to 0.003125T and in the mean time extend internal iteration cycles for wave periods of 6 and 8 seconds to ensure solution quality. In these cases, simulations were conducted for 20,000 time step. The duration remains 62.5 wave cycles as the time increment was cut to one half. Results are presented in [Figures 21](#) through [27](#).

In general, adding the proposed south breakwater substantially mitigates wave turbulences in the basin. But the resulting layout still admits much higher waves than preferred (USACE, 2003)<sup>9</sup> through multiple paths around the additional barrier. Take incident waves approaching from 0 degree heading for example. The new basin entrance now faces in a direction perpendicular to the wave heading. Intuitively, the incident waves are supposed to reflect off the south breakwater or the main bulkheads and return to the open water. Indeed, most of the waves do. However, substantial waves still enter the basin via diffraction around the south breakwater or lateral transmissions powered by water surface gradient across the basin entrance ([bkwt\\_eff\\_0040a.avi](#)). [Figure 21](#) indicates that two breakwaters combined cut wave heights inside the basin by 70% from the present level with the north breakwater alone ([Figure 12](#)). Yet, much of the deep water area still observes transmission coefficients of 0.2 to 0.3. This seems higher than the fair share contribution by diffraction alone. For instance, an analytical solution for wave diffraction around a semi-infinite barrier by Wiegel (1962) as shown in [Figure 22](#)<sup>10</sup> predicts a diffraction coefficient of 0.15 at three wave lengths along the radius at 45 degrees inside the geometric shadow. Possible causes may be traced back to the significant standing waves at the main bulkheads and breakwaters. Waves outside the basin with the presence of the south breakwater are in general higher than those before the breakwater was installed ([bkwt\\_eff\\_0040b.avi](#)). This stages a greater surface gradient across the entrance than that appears in the theoretical case of [Figure 21](#) and thus thrusts a higher wave transmission. Besides, waves creeping through the 30-foot gap at the root of the south breakwater also impose substantial contribution. The present simulation suggests a transmission coefficient of 10% attributable to this source at one wave length from the gap ([5t043c3d.avi](#)). It is believed that diffraction around the north end of the south breakwater prevails and sets the tone of concentric wave pattern between two breakwaters. The other two components moderately revise the pattern and add the appearance of ring waves. The resulting waves further propagate into the basin directly or around the north breakwater. Note the intruding waves are now oblique to the south bulkhead. It is reasonable that the consequence of wave reflections sustains relatively higher intensities along the south bulkhead. The wave pattern is obviously more complicated than before the south breakwater was installed. However, the conditions

---

<sup>9</sup> Standard operational criteria used by US Army Corps of Engineers requires wind waves and swells in small-craft harbors near the berthing areas not exceeding one foot more than 10 percent of the time.

<sup>10</sup> See Shore Protection Manual, 1984. PP 2-83.

inside the basin are substantially improved by cutting off the direct wave source through the existing basin entrance. Standing waves at the east bulkhead are still noticeable. This explains the relatively high waves at the east basin.

Figure 25 summarizes the performances of the proposed layout in local storms. Details of wave paths and wave activities are documented in the attached movie clips. Generally speaking, this layout works fairly well in perpendicular waves, but gradually loses its effectiveness as the incident waves swing toward the northwest. This should not be a surprise since the oblique waves are better aligned with the new entrance and able to find direct paths into the basin. Besides, comparable amounts of incident waves outside the window of direct paths are guided into the basin by the breakwaters. These two sources overpower diffractions around the south breakwater as indicated by the straight and parallel wave crests between breakwaters. Most importantly, these intruding waves are subsequently reflected by the south bulkhead to enhance the wave turbulences in the back side of the basin. Figure 21 suggests that two breakwaters combined cuts the wave disturbances inside the basin by 70% from the present level in perpendicular waves. The reduction drops to 50% in 22.5-degree waves (Figure 23) and 20% in 45-degree waves (Figure 24). Bear in mind that these statistics gauge the breakwater performance in a relative sense by the extent of turbulence reduction from the present level of respective ambient waves. By this standard, the present breakwater layout is less effective in oblique seas. Figures 23 and 24 indicate that this basin with the south breakwater may observe at least the same level of wave turbulence as the incident waves along the south bulkhead in oblique seas. Similarly, the wave turbulences are around 20% of the incident waves at the north basin and 35% at the east basin. However, the actual levels of wave turbulences are of more significance to basin design and operation. Since waves induced by local storms in this area are essentially linear, the actual wave heights in the basin may be obtained by multiplying the transmission coefficients by the true incident wave heights. In the case of Sea State 3<sup>11</sup> for instance, wave conditions at Zone B and Zone C are marginal by the standard of the Army Corps of Engineers<sup>9</sup>, while Zone A is apparently overly exposed.

Figures 26 and 27 are examples of wave distributions in the basin after adding the south breakwater in the 6- and 8- second waves, respectively. The wave disturbances are significantly reduced. Maxima decrease to 35% along the south bulkhead and 25% in the east basin at the instant. The breakwater performances in various wave lengths are further summarized in Figure 28. The top row reiterates the wave activities in the basin as is, while the bottom row summarizes the results after the addition of the south breakwater. It can be seen that the differences in wave paths and wave patterns before and after adding the south breakwater in longer waves are similar to the observations in the 4-second waves, with the exception that the diffractions reach farther because the basin appears smaller relative to the longer waves. As a result, longer waves induce higher wave disturbances in the basin. However, the breakwaters cut the wave turbulences inside the basin by a similar amount of 50% over all from the level with the north breakwater alone for all perpendicular waves after correction of refraction effects<sup>12</sup> as shown in Figures 21, 26 and 27 and the movie clips [bkwt\\_eff\\_40b.avi](#), [bkwt\\_eff\\_60.avi](#), and [bkwt\\_eff\\_80.avi](#).

---

<sup>11</sup> Significant wave height varies from 3 to 5 feet and peak period is around 5 seconds.

<sup>12</sup> See discussions on Page 22.

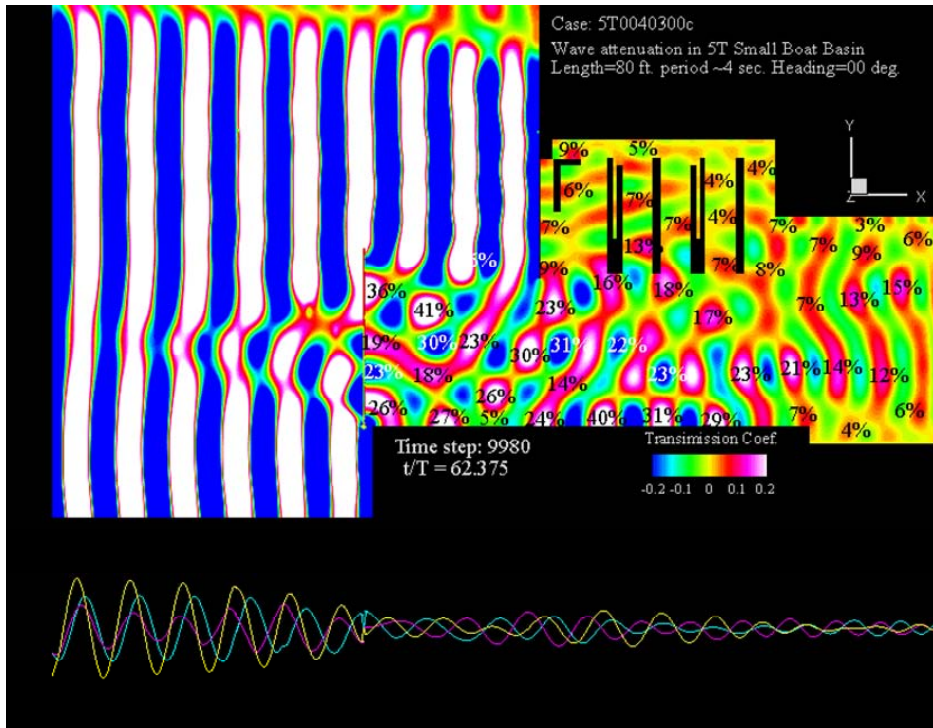
As observed in series one that longer waves penetrate the basin more effectively. Similar trend retains after adding the south breakwater (Figure 29). However, the nature of excitations looks different. With this addition, incident waves trigger a resonance-like oscillation in the space between two breakwaters. This behavior is not seen before adding the south breakwater. The simple patterns of 8-second waves render the disparities more visible ([bsnosl\\_a.avi](#)). Figure 30 is a snap shot of this activity near the peak. While the top row shows the wave patterns with and without the south breakwater, the three frames at the bottom demonstrate wave profiles across the basin at three locations along the major axis. These are free water surface profiles observed from inside the basin toward the entrance. As a result, the lower ends of these profiles are touching the south bulkhead. Frame (c), in particular, illustrates the intense resonance-like profile (red) just inside the south breakwater as opposed to the progressive wave array (cyan) in absence of the breakwater. In the latter case, the entire profile fluctuates in sync with some lateral oscillations, reflecting the phase difference between two standing wave systems at the main bulkheads across the basin entrance. These natures propagate down the basin to sections (d) and (e). Note that this breakwater happens to be of the same length as the 8-second waves, or roughly two and four times of the 6- and 4- second waves. The shorter waves also induced similar oscillations as seen in Figures 31 and 32 with the exception that their profiles resemble the higher harmonics of their respective wave lengths. Figure 33 further summarizes their nature and their sensitivity to the incident wave lengths. It is obvious that longer waves induce stronger responses as previously seen. A closer review of the associated movie, [bsnosl\\_b.avi](#) for instance, further reveals some subtle differences in addition to the wave lengths and intensities. Basically, the 8-second profile exhibits a clear standing oscillation from the early stage. The 4-second profile, on the other hand, shows much of progressive nature initially and gradually settles in standing oscillations at the middle of the south breakwater, while the profiles at both ends retain heavy progressive flavor. The 6-second profile is a mixture of both. These oscillations in turn pump wave arrays down the basin as shown by the longitudinal profiles (Frame (e)). Another obvious scene is the distinct wave patterns in three respective zones of the basin as shown in Figure 7c. Note that each of these three zones roughly describes a rectangular sub-basin of unique depth characteristics. The intruding waves sweep through Zone A like a progressive array and subsequently evolve into a clear circulating pattern in Zone C. Zone B, on the other hand, presents a progressive wave array perpendicular to the incident waves due to diffractions and clear resonances in both principal directions. Again the width of Zone B is comparable to the 8-second waves. In fact, these three patterns exist regardless of the presence of the south breakwater. Apparently, they are the intrinsic features of this basin.

Figure 34 compares wave activities with (top right) and without (top left) the south breakwater in 8-second waves. Three wave profiles were extracted from each case at exactly the same cross sections through the basin as illustrated. These profiles are laid against each other in the bottom chart in bird's-eye view from 45 degrees above the horizon. The profiles at the same locations are presented in like colors with the case without the south breakwater in darker tones. Movie clip [5t083d4va.avi](#) captures the time histories of these profiles. In addition to the anticipated wave mitigation and the intense resonance near the basin entrance, the wave enhancements near the east bulkhead are of

practical interest. This movie clearly illustrates the process a progressive wave array evolving into standing waves against vertical walls. Movie clip [5t083d4vb.avi](#), which traces consecutive wave profiles at exactly one wave cycle apart, further indicates that their amplitudes actually oscillate in time. The range of oscillation is in the order of 5 to 10 percents of the wave heights. Furthermore, the wave lengths in the basin after adding the south breakwater are noticeably shorter than their counterparts before adding the south breakwater. A simplified analysis indicates that the wave lengths before adding the south breakwater are close to the wave lengths at the local water depths predicted by linear wave theories while the wave lengths after adding the breakwater are closer to the basin oscillations. [Figures 35](#) and [36](#) are similar views in 6- and 4-second waves. The associated movie clips indicate that standing wave patterns are less complete in the case of 6-second waves and almost invisible in the 4-second waves, perhaps due to higher dispersions. Although height amplifications are clearly seen, the shorter waves present more of progressive natures ([standing waves.avi](#)).

Although the present observation is far from conclusive, evidence indicates that reconfiguring the basin and breakwater layouts may change the nature of driving forces and the hydrodynamic responses in the basin. Their impact to the basin operations is a subject for consideration at the early stage of design and planning.

The series of floating docks and the fuel pier at the north basin are critical assets to small boat operations. This water area is primarily protected by the north breakwater from local storms and experiences mild wave disturbances most of the time. [Figure 37](#) provides a brief overview of the local wave activities at the present in various ambient wave conditions. It can be seen that excessive waves can reach this area in oblique seas. Besides, swells of 8 seconds or longer may also excite this water beyond the operational criteria for small boats at piers. [Figure 38](#) indicates that the south breakwater as proposed offers additional protection to the north basin. Nevertheless oblique seas continue to be a concern after adding the south breakwater.



5T043c.avi

5T043c3D.avi

Figure 21. Wave distribution with the south breakwater (4 sec, 00 deg).

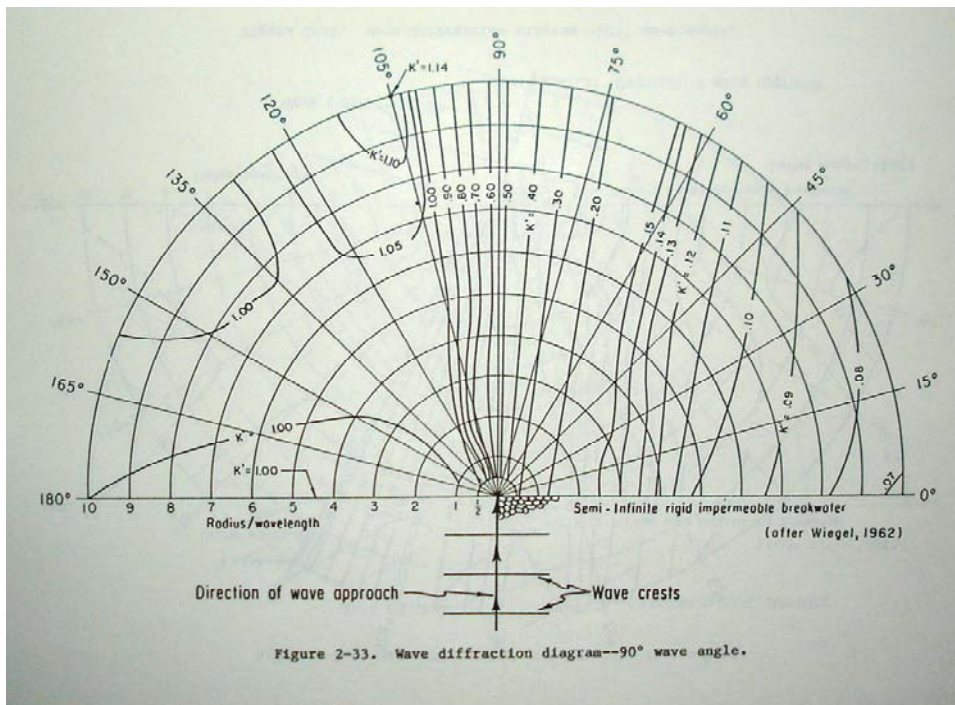
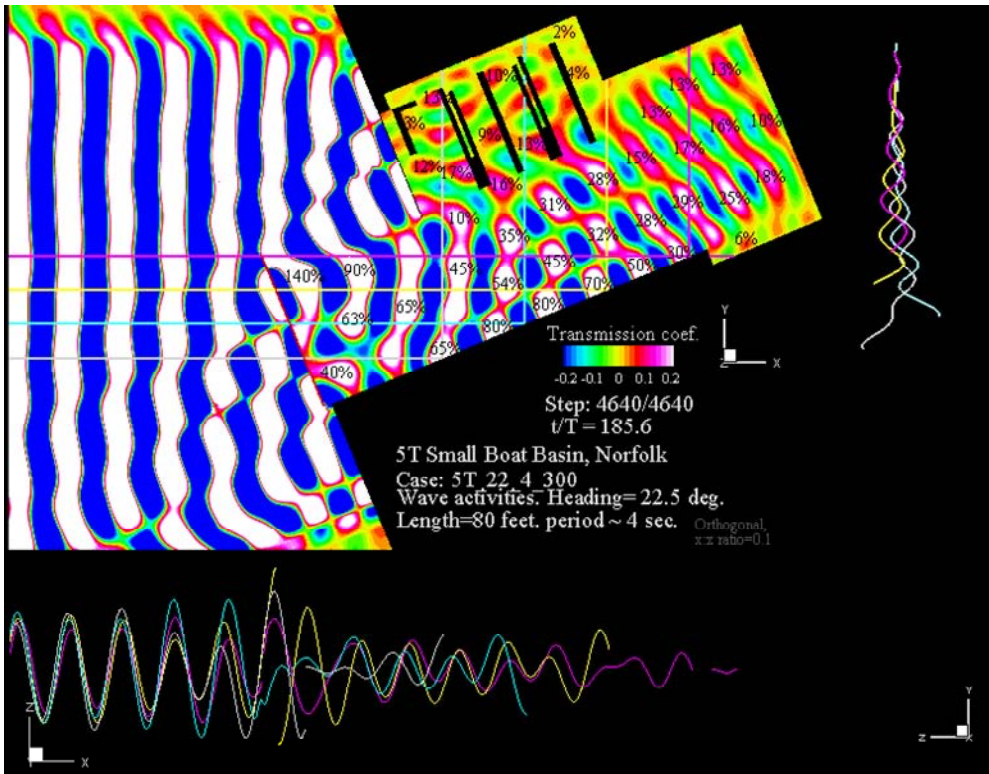


Figure 22. Diffraction diagram around a semi-infinite barrier (Excerpted from Shore Protection Manual, 1984, Page 2-98).

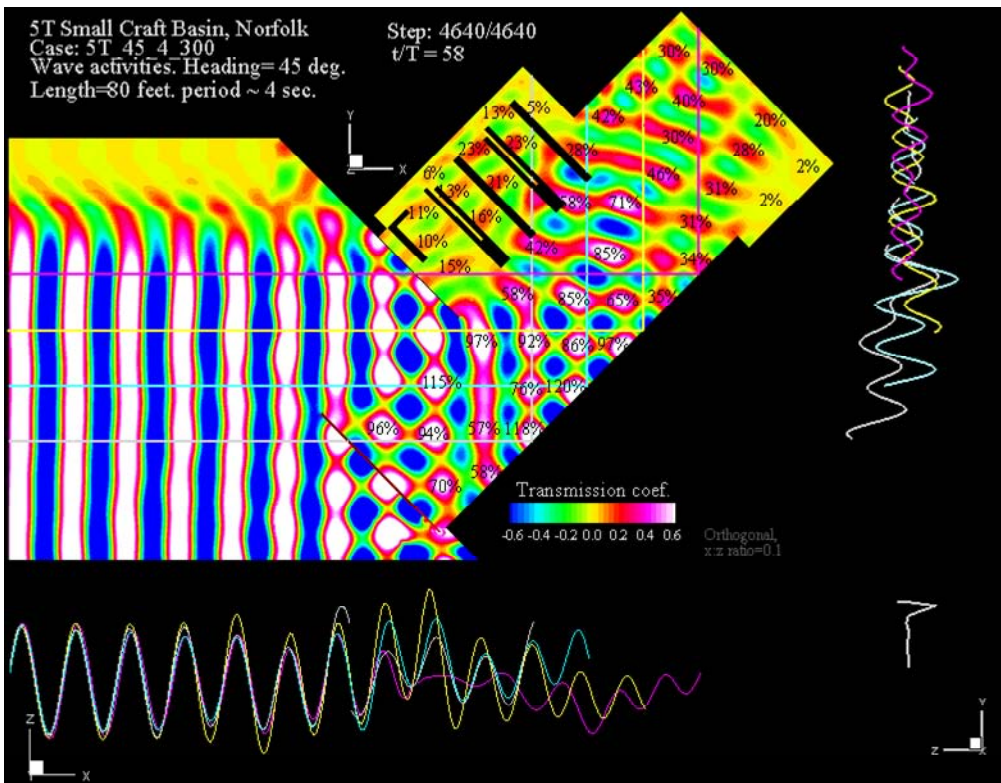




5T243a.avi

5T243b.avi

Figure 23. Wave distribution with the south breakwater (4 sec, 22.5 deg).

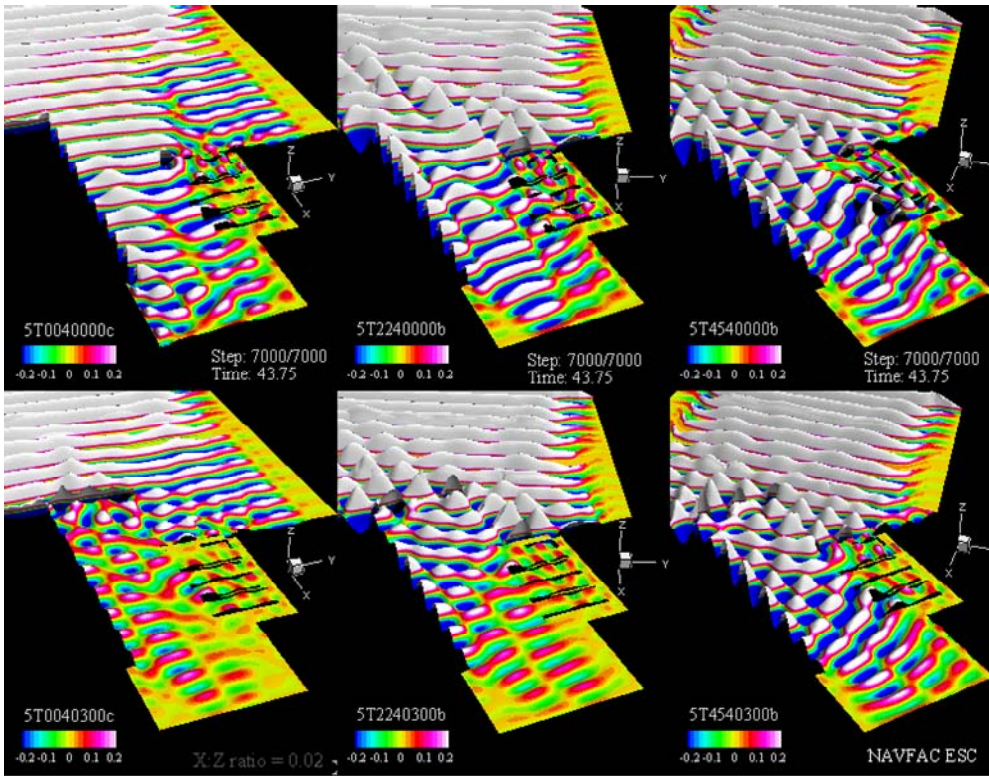


5T443.avi

5T443Da.avi

5T443Db.avi

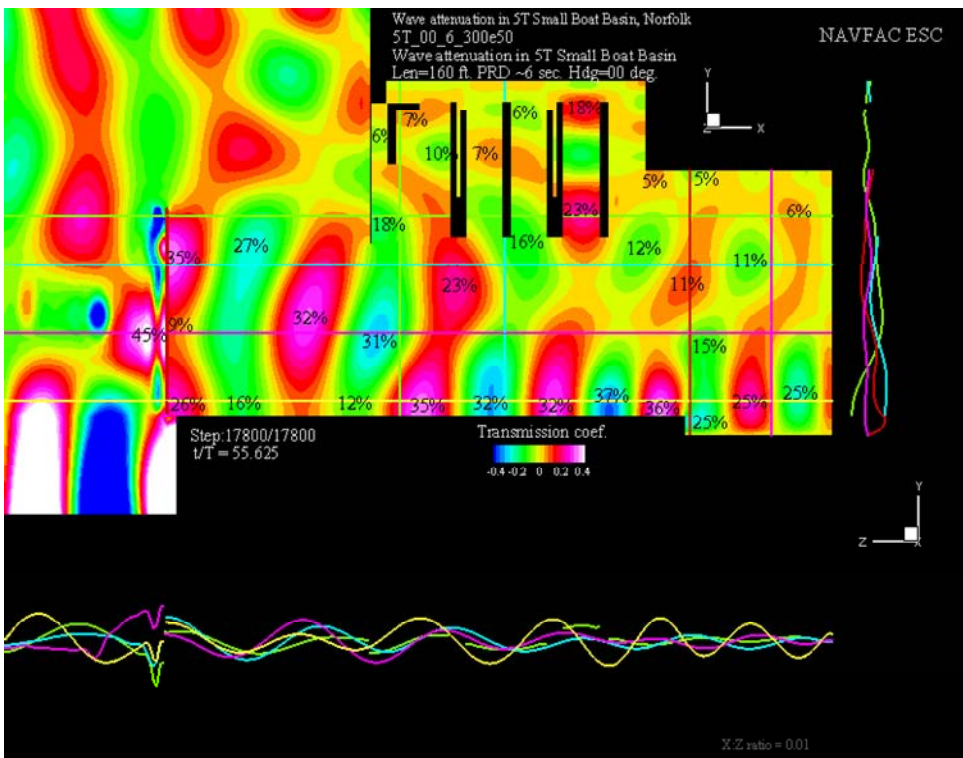
Figure 24. Wave distribution with the south breakwater (4 sec, 45 deg).



hdg\_sum1.avi

hdg\_sum2.avi

Figure 25. Summary of breakwater performances in local storms.



5T063e50a.avi  
 5T063e3D.avi  
 5T063e50c.avi  
 5T063e50d.avi

Figure 26. Wave distributions with the south breakwater (6 sec. 00 deg).



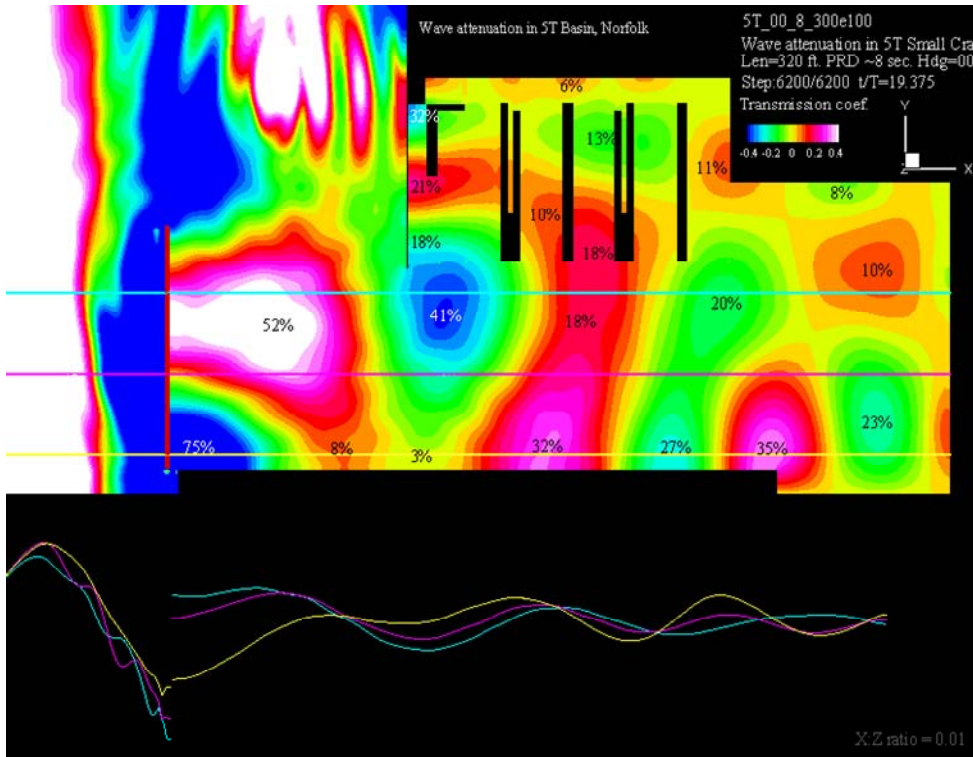


Figure 27. Wave distributions with the south breakwater (8 sec. 00 deg).

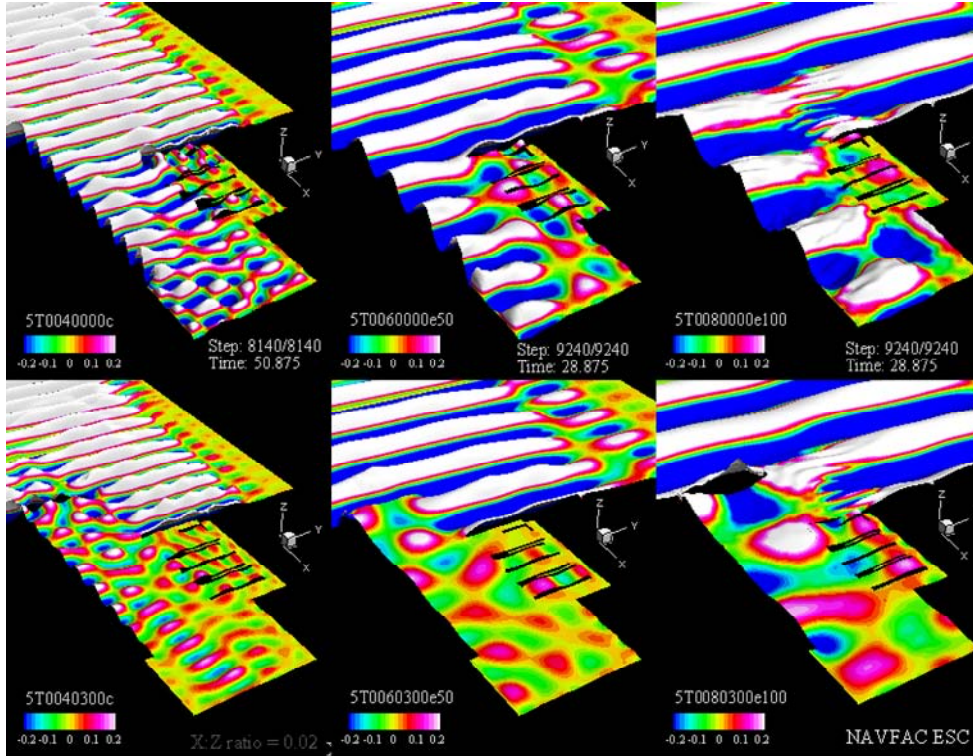
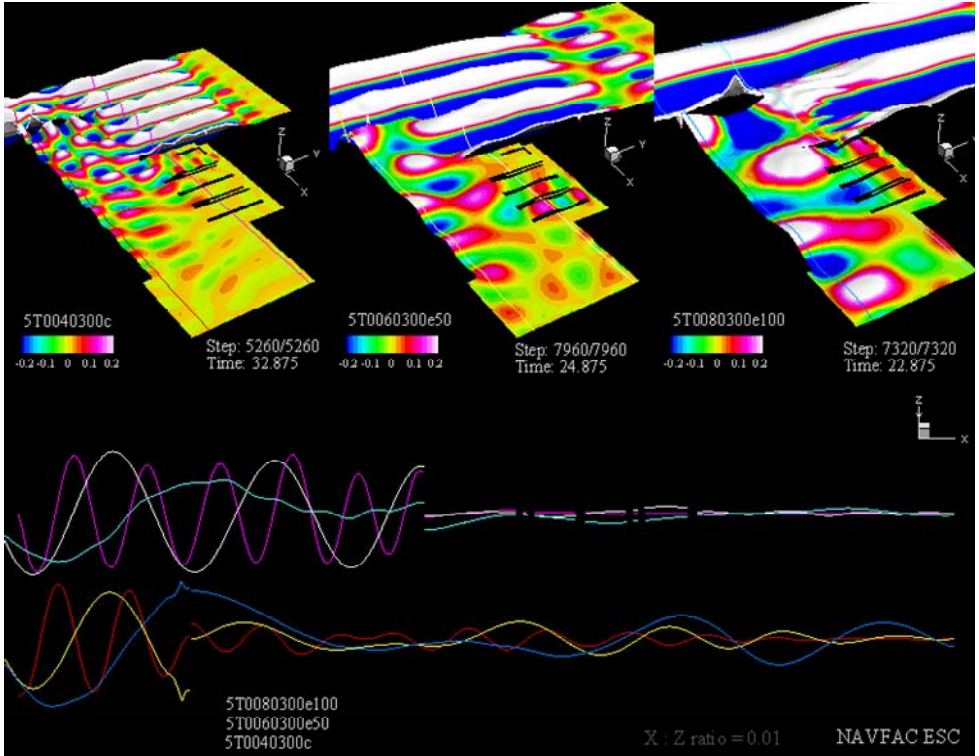
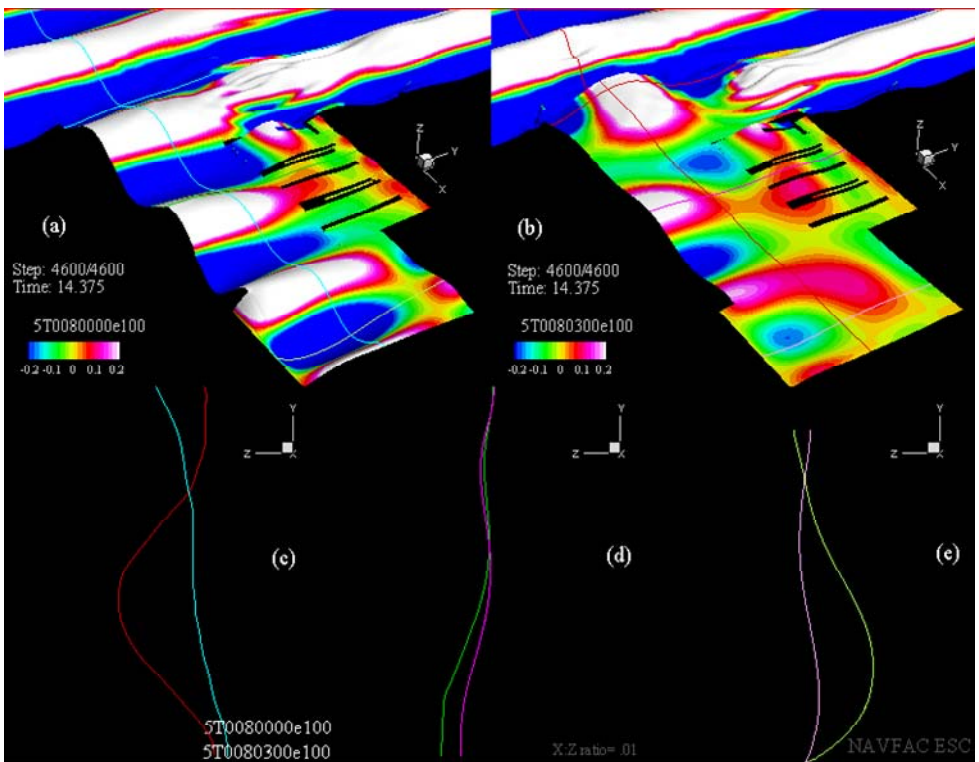


Figure 28. Sensitivity of breakwater performance to wave lengths.



cmpr\_prof\_bk  
wat\_prd.avi

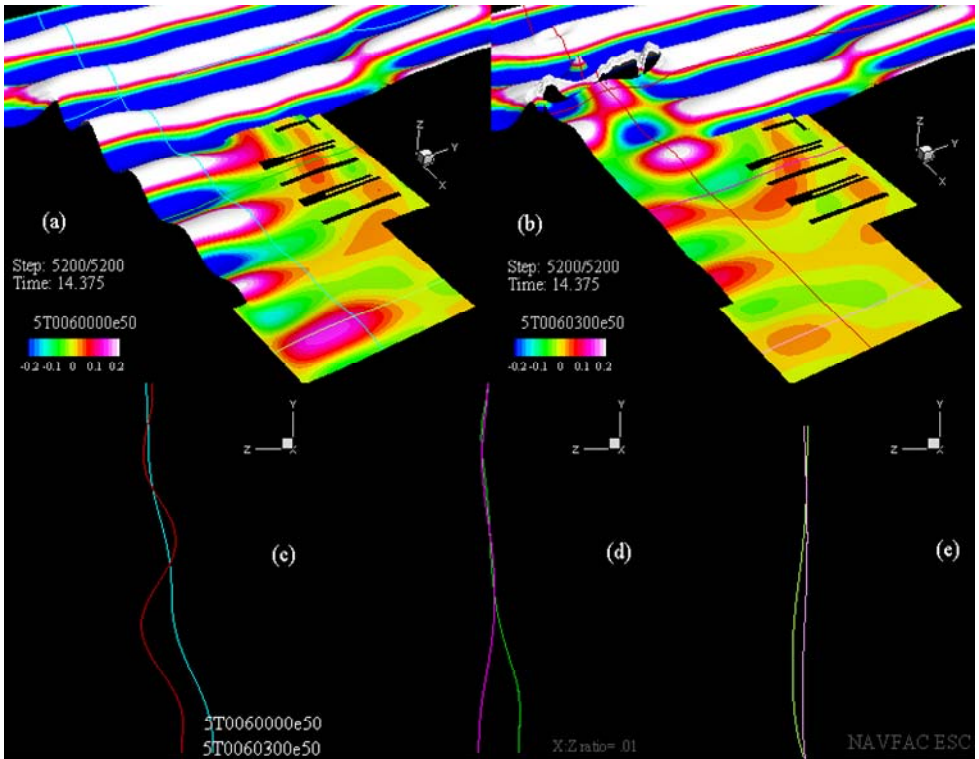
Figure 29. Sensitivity of wave lengths with the south breakwater.



bsnosl\_8a.  
avi

bsnosl\_8b.  
avi

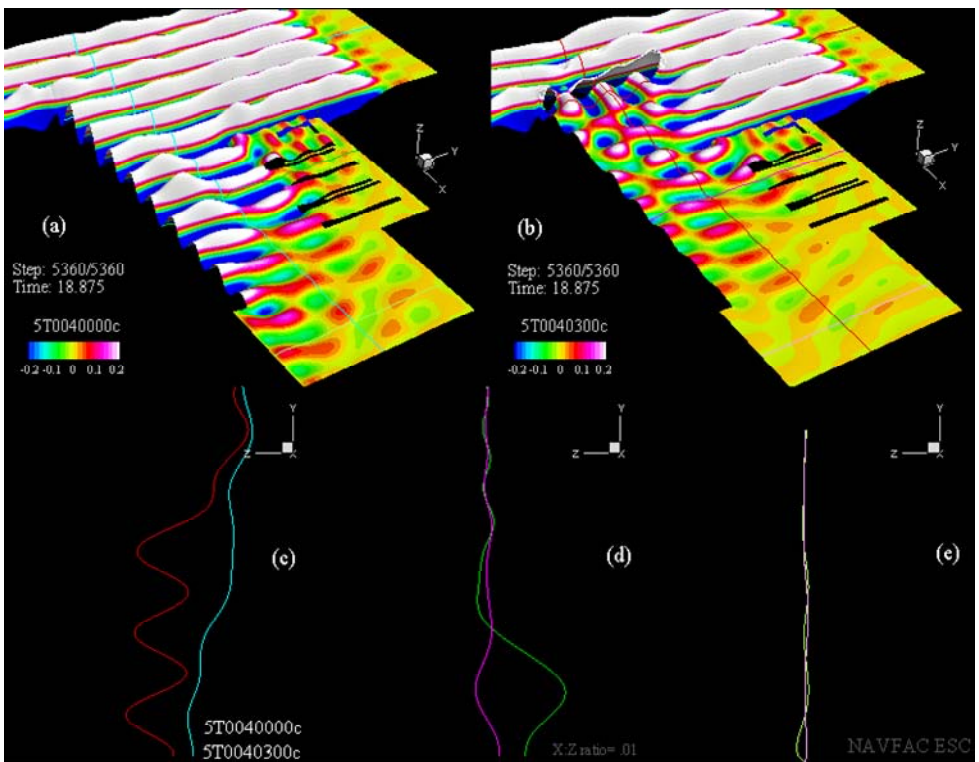
Figure 30. Resonance-like waves behind the south breakwater (8-sec).



bsnosl\_6a.  
avi

bsnosl\_6b.  
avi

Figure 31. Resonance-like waves behind the south breakwater (6 sec).



bsnosl\_4a.  
avi

bsnosl\_4b.  
avi

Figure 32. Resonance-like actions behind the south breakwater (4 sec).



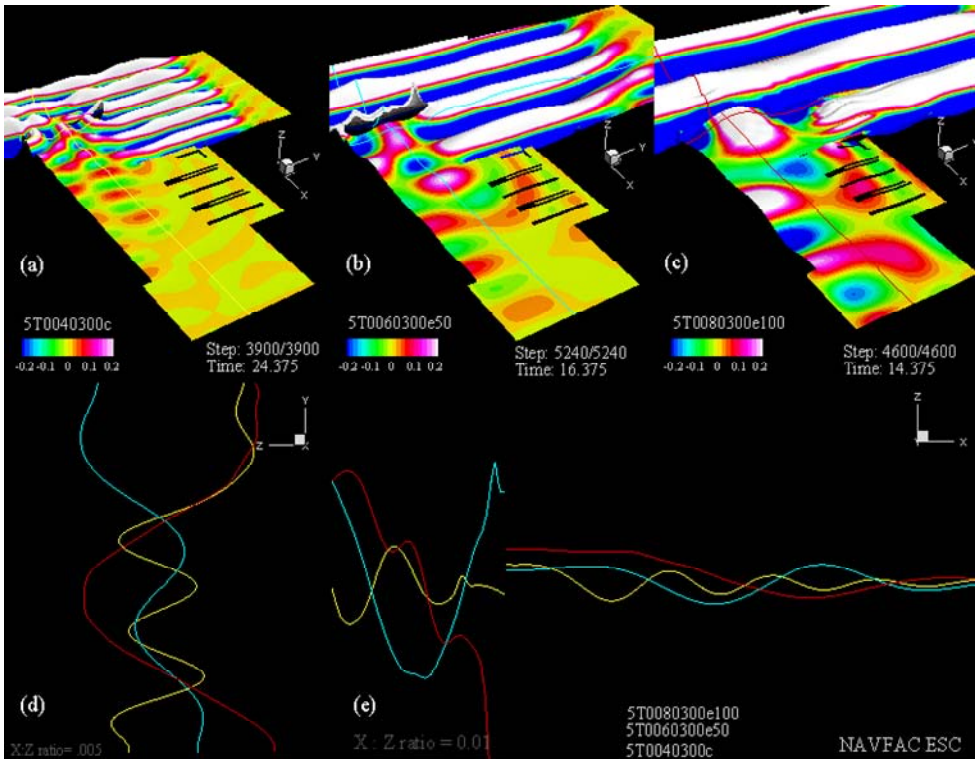


Figure 33. Sensitivity of resonance-like oscillations to wave periods. .

bsnosl\_prd  
.avi  
bsnosl\_b.a  
vi

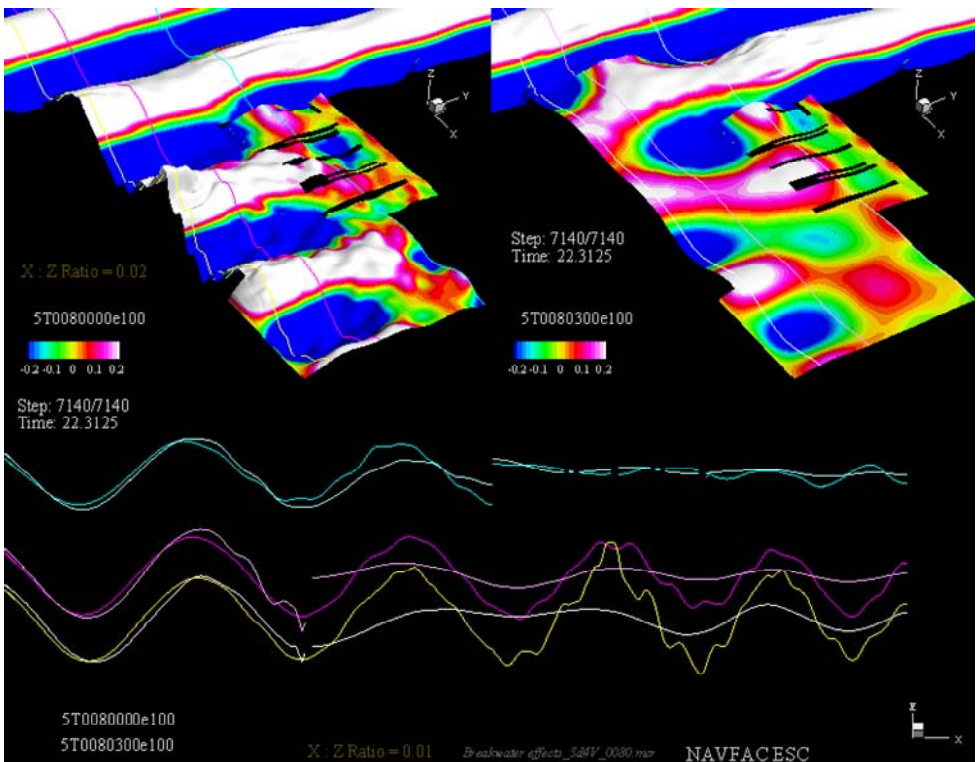
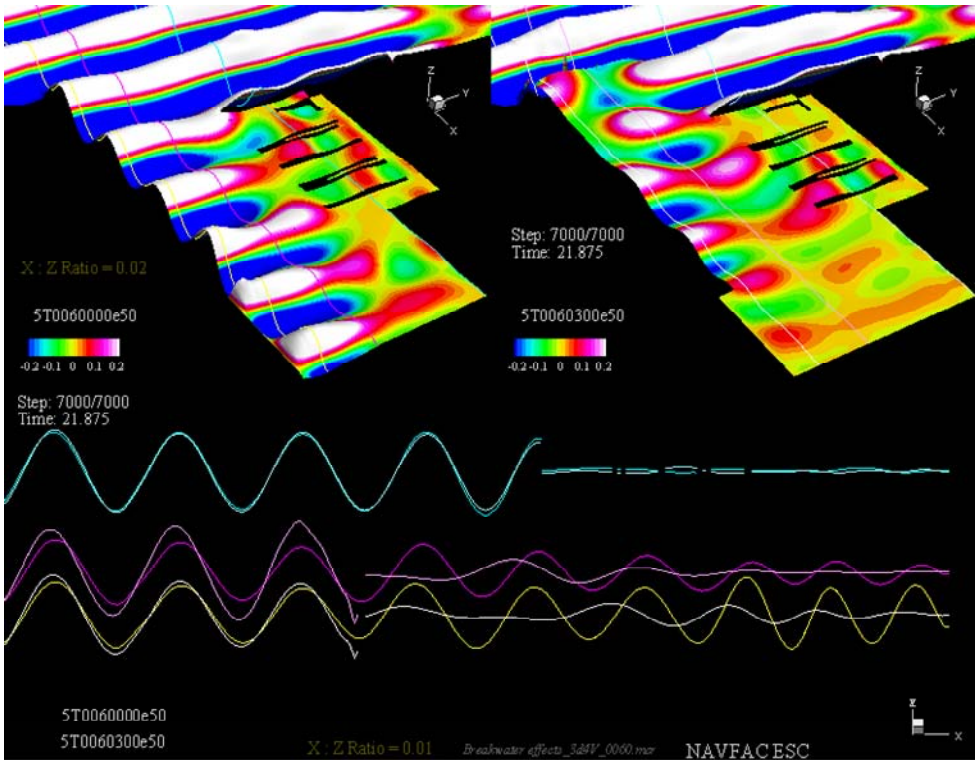


Figure 34. Breakwater changes wave nature in the basin (00 deg. 8 sec.).

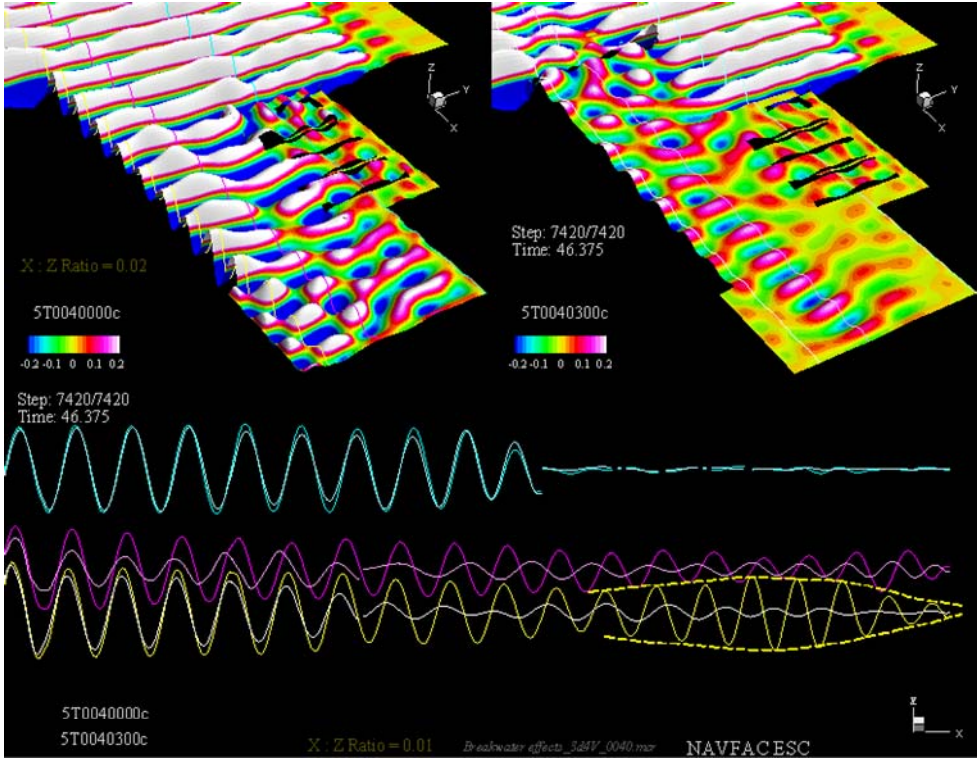
5T083D4va.av  
i  
5T083d4vb.av  
i



5T063d4va.av  
i

5T063D4vb.a  
vi

Figure 35. Breakwater changes wave nature in the basin (00 deg. 6 sec.).

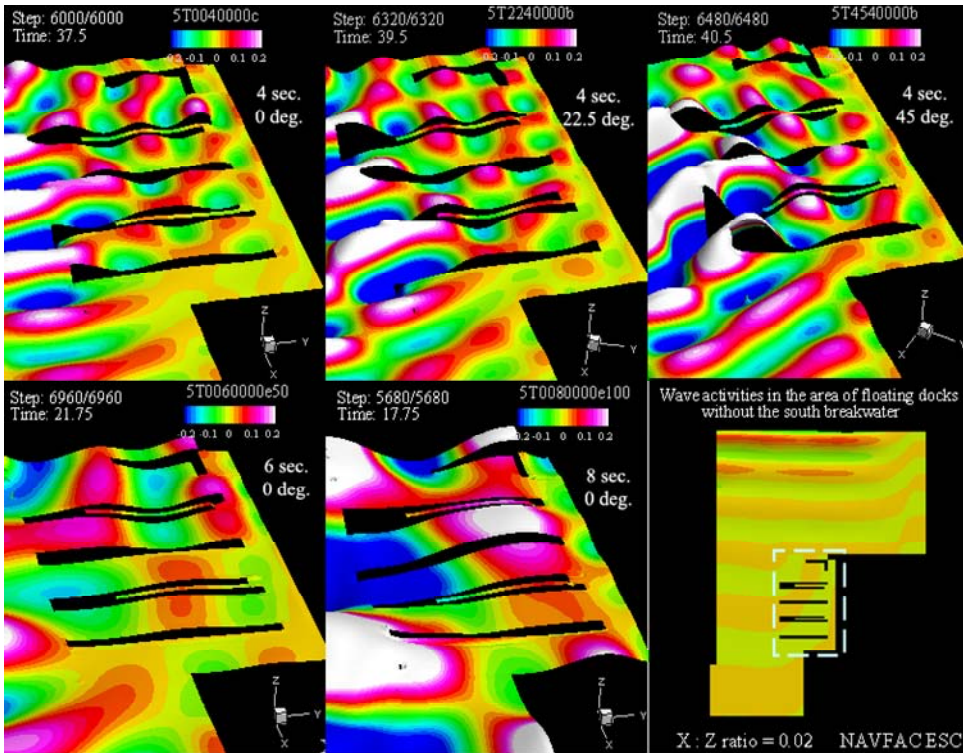


5T043D4va.av  
i

5T043d4vb.av  
i

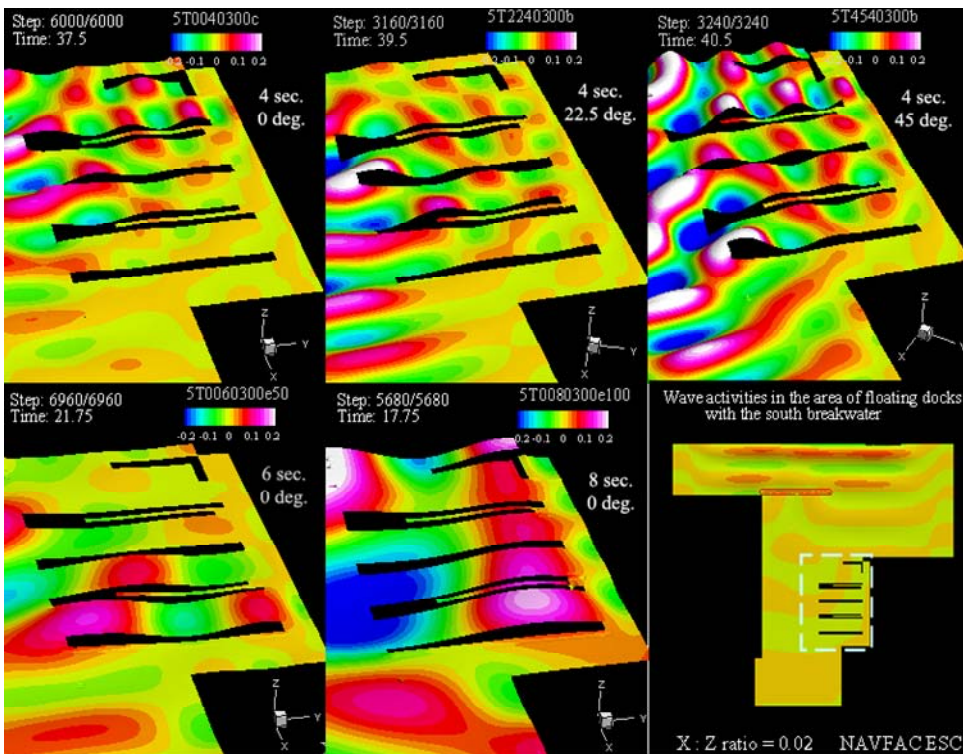
Figure 36. Breakwater changes wave nature in the basin (00 deg. 4 sec.).





docks\_open.av  
i

Figure 37. Wave activities near the floating docks (without south breakwater).

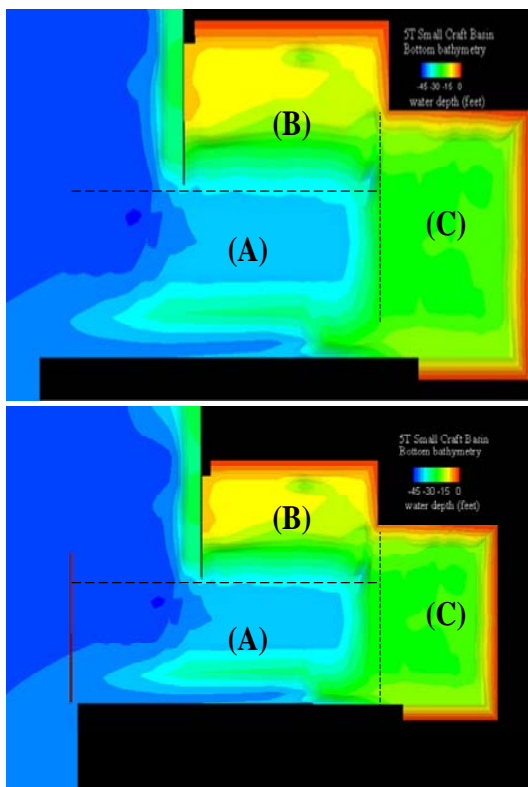


5T043D4va.av  
i  
5T043d4vb.av  
i

Figure 38. Wave activities near the floating docks (with south breakwater).

## SUMMARY

This effort determined the dynamic responses of a small boat basin to local storms and evaluated the performance of a proposed breakwater. The evaluation was conducted with a simulation model capable of precisely addressing the exact site conditions and faithfully preserving all hydrodynamic mechanisms at high accuracy. The results clearly delineate the paths of wave propagation and the wave fields inside the basin. Table 1 provides a synoptic summary of the wave disturbances in the basin before and after the implementation of the south breakwater. For convenience, this basin is divided into three zones by depth. The wave disturbances are shown in terms of transmission coefficients (K), or the ratio of local wave height to the prescribed wave height at the wavemaker. Note that K values in this table are listed in percentage.



<b>Before adding the south breakwater</b>			
K (%)	A (%)	B(%)	C(%)
heading	wave period = 4 seconds		
0	45~90/70	15 ~ 35	30 ~ 60
22.5	60 ~ 145	15 ~ 30	20 ~ 80
45	70 ~ 150	30 ~ 60	20 ~ 70
	wave period = 6 seconds		
0	20 ~ 80	10 ~ 25	15 ~ 60
	wave period = 8 seconds		
0	50 ~ 180	10 ~ 25	20 ~ 110
<b>After adding the south breakwater</b>			
K (%)	A(%)	B(%)	C(%)
heading	wave period = 4 seconds		
0	20 ~ 30	5 ~ 15	5 ~ 15
22.5	30 ~ 80	10 ~ 15	10 ~ 30
45	50 ~ 120	10 ~ 25	20 ~ 40
	wave period = 6 seconds		
0	10 ~ 35	5 ~ 20	5 ~ 25
	wave period = 8 seconds		
0	20 ~ 40	10 ~ 20	10 ~ 35

Table 1. Summary of wave disturbances before and after adding the south breakwater (from Figures 12, 16, 17, 18, 19, 21, 23, 24, 26, and 27).

Findings pertaining to the dynamic nature of this basin and the performance of the proposed breakwater are briefly summarized as follows.

- (a) This basin is sensitive to local storms. It is particularly susceptible to oblique waves from the northwestern quadrant. The north breakwater alone is insufficient to shelter the basin.

- (b) Wave patterns inside the basin are complex. Paths of intrusion vary with wave characters, such as lengths and headings. The south bulkhead is critical to the wave activities inside the basin. This straight vertical wall is partly exposed to the oblique waves and reflects the intruding waves like a mirror. The high wave disturbances in the north half of the basin are mostly linked to this bulkhead. The intruding waves further trigger cross basin resonances and set up standing waves at the bulkheads. These induced waves are important ingredients to the free surface complexities inside the basin.
- (c) The addition of the south breakwater substantially mitigates wave disturbances in the basin. Two breakwaters combined cuts the present wave disturbances with the north breakwater alone by 30% to 70%, depending on wave periods and headings. By this standard, this breakwater layout works reasonably well in perpendicular waves from west southwest and gradually loses its effectiveness as the incident waves shifts toward northwest. However, it is more practical to measure the breakwater performance by its ability to maintain wave disturbances inside the basin under a tolerable level determined by basin operations.
- (d) The US Army Corps of Engineers recommends an operational standard for small boat harbors that wind-induced waves near berthing areas shall not exceed one foot more than 10 percent of the time. By this standard, the area of floating docks is duly sheltered up to Sea State 3 with the addition of the south breakwater. The waters near the 5T Pier are marginal in perpendicular waves of high Sea State 2, but are overly exposed to oblique seas.

## RECOMMENDATIONS

It is understood that a proper design shall observe site constraints and meet prescribed criteria. However, two simple measures that may substantially mitigate wave disturbances inside the basin deserve consideration.

- (a) Extend the south breakwater and bend its north end by 45 degrees to the east as shown by the dash line in [Figure 39](#). This would reduce the amount of oblique waves penetrating through the basin entrance. In fact, the south breakwater need not be straight or parallel to the north breakwater. A zigzag shape may be more favorable from the consideration of basin stability.
- (b) Install wave absorbing mechanisms along the south bulkhead as well as the weather side of the north breakwater and perhaps the leeward side of the south breakwater, as shown by the boxes in [Figure 39](#). This would reduce wave intrusions via successive reflections off the breakwaters. More importantly, this would reduce the intruding waves from reflecting into the basin and thus mitigate cross basin oscillations and wave disturbances.

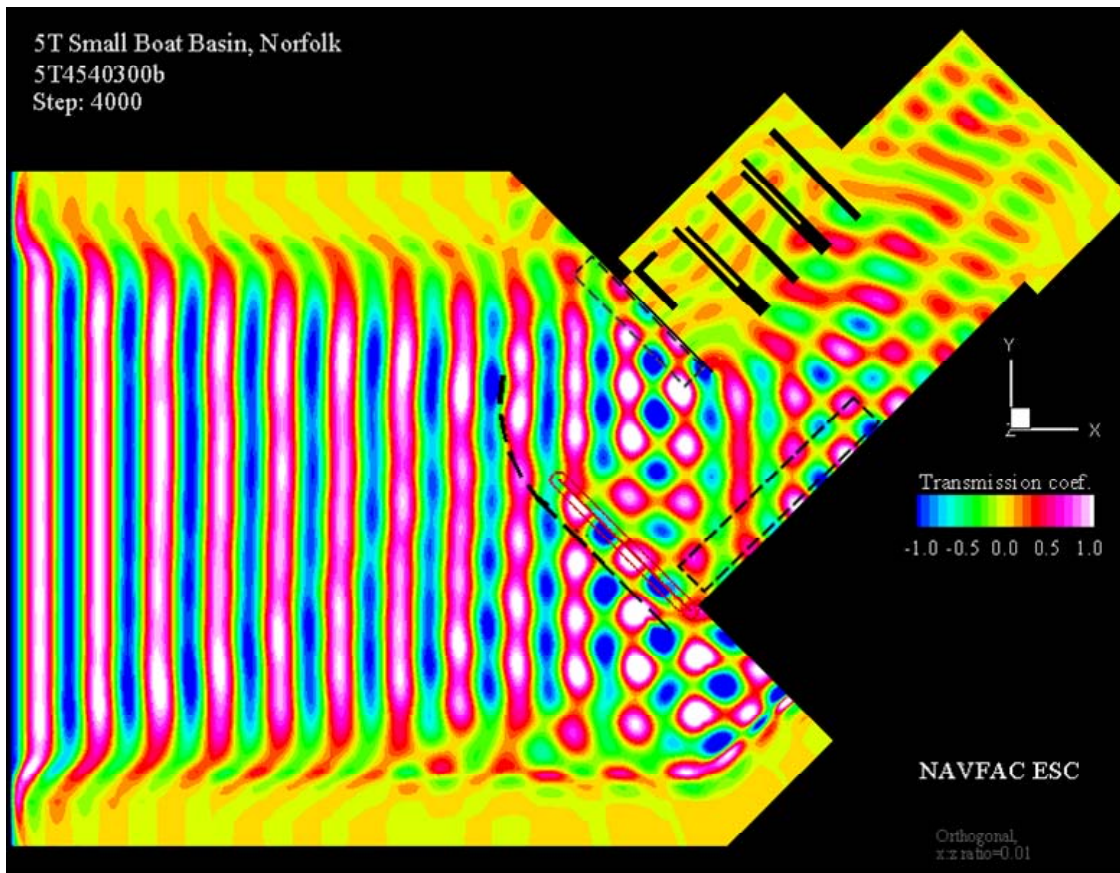


[Figure 39](#). Potential measures to mitigate wave activities inside the basin.



## REFERENCES

Chen, H.C. and Lin, W.M. (1998), "Numerical Simulation of Wave Effects on a Combined Breakwater and Floating Platform Configuration," Proceedings of 1998 International OTRC Symposium on Ocean Wave Kinematics, Dynamics and Loads on Structures, pp. 116-125, Houston, TX.

Chen, H.C. and Lin, W.M. (2000), "Numerical Simulation of Wave Effects around Compound Coastal Structures," Journal of Visualization, Vol. 3, No. 3, pp. 287-294.

Chen, H.C. and Liu, T.L. (2001), "Numerical Simulation of Shallow Water Nonlinear Waves Around Coastal Structures by a Chimera Potential-Flow Method," 11th International Offshore and Polar Engineering Conference, Vol. III, pp. 205-212, Stavanger, Norway.

Chen, H.C., Patel, V.C., and Ju, S. (1990), "Solutions of Reynolds-Averaged Navier-Stokes Equations for Three-Dimensional Incompressible Flows," Journal of Computational Physics, Vol. 88, No. 2, pp. 305-336.

Clement, A. (1996), "Coupling of Two Absorbing Boundary Conditions for 2D Time-Simulations of Free Surface Gravity Waves," Journal of Computational Physics, Vol. 126, pp. 139-151.

Dalrymple R.A. and Martin, P.A. (1996), "Water Waves Incident on an Infinitely Long Rectangular Inlet," Applied Ocean Research, Vol. 18, pp. 1-11.

Huang, E.T. and Chen, H.C. (2003), "Ship Berthing at a Floating Pier," 13th International Offshore and Polar Engineering Conference, Vol. III, pp. 683-690, Honolulu, Hawaii.

Kang, C.H., Chen, H.C. and Huang, E.T., "Chimera RANS/LAPLACE Simulation of Free Surface Flows Induced by 2D Ship Sway, Heave, and Roll Motions," Proceedings, 8th International Offshore and Polar Engineering Conference, Vol. III, pp. 320-327, Montreal, Canada, May 24-29, 1998.

US Army Corps of Engineers (1984), "Shore Protection Manual," Waterways Experiment Station, PO Box 631, Vicksburg, MS 39180

US Army Corps of Engineers (2003), "Coastal Engineering Manual," EM-1110-2-1100, Department of the Army, USACE, Washington, DC 20314-1000, Part V, Chap 5, pp V-5-74

Vincent, C.L. and Briggs, M.J. (1989), "Refraction-Diffraction of Irregular Waves Over a Mound," Journal of Waterway, Port, Coastal, and Ocean Engineering, Vol. 115, pp. 269-284.

Wiegel, R. L, "Oscillatory Waves," U. S. Army, Beach Erosion board, Bulletin, Special Issue No. 1, July 1948.